2004

Sterol Carrier Protein-2 Directly Interacts with Caveolin-1 in Vitro and in Vivo

Minglong Zhou
Texas A & M University - College Station

Rebecca D. Parr
Stephen F Austin State University, parrrl@sfasu.edu

Anca D. Petrescu
Texas A & M University - College Station

H. Ross Payne
Texas A & M University - College Station

Barbara P. Atshaves
Texas A & M University - College Station

See next page for additional authors

Authors
Minglong Zhou, Rebecca D. Parr, Anca D. Petrescu, H. Ross Payne, Barbara P. Atshaves, Ann B. Kier, Judith M. Ball, and Friedhelm Schroeder

Sterol Carrier Protein-2 Directly Interacts with Caveolin-1 in Vitro and in Vivo†

Minglong Zhou,‡ Rebecca D. Parr,§ Anca D. Petrescu,‡ H. Ross Payne,§ Barbara P. Atshaves,‡ Ann B. Kier,§ Judith M. Ball,§ and Friedhelm Schroeder*,‡

Department of Physiology and Pharmacology, Texas A&M University, TVMC, College Station, Texas 77843-4466, and Department of Pathobiology, Texas A&M University, TVMC, College Station, Texas 77843-4467

Received October 27, 2003; Revised Manuscript Received March 10, 2004

ABSTRACT: HDL-mediated reverse-cholesterol transport as well as phosphoinositide signaling are mediated through plasma membrane microdomains termed caveolae/lipid rafts. However, relatively little is known regarding mechanism(s) whereby these lipids traffic to or are targeted to caveolae/lipid rafts. Since sterol carrier protein-2 (SCP-2) binds both cholesterol and phosphatidylinositol, the possibility that SCP-2 might interact with caveolin-1 and caveolae was examined. Double immunolabeling and laser scanning fluorescence microscopy showed that a small but significant portion of SCP-2 colocalized with caveolin-1 primarily at the plasma membrane of L-cells and more so within intracellular punctuate structures in hepatoma cells. In SCP-2 overexpressing L-cells, SCP-2 was detected in close proximity to caveolin, 48 ± 4 Å, as determined by fluorescence resonance energy transfer (FRET) and immunogold electron microscopy. Cell fractionation of SCP-2 overexpressing L-cells and Western blotting detected SCP-2 in purified plasma membranes, especially in caveolae/ lipid rafts as compared to the nonraft fraction. SCP-2 and caveolin-1 were coimmunoprecipitated from cell lysates by anti-caveolin-1 and anti-SCP-2. Finally, a yeast two-hybrid assay demonstrated that SCP-2 directly interacts with caveolin-1 in vivo. These interactions of SCP-2 with caveolin-1 were specific since a functionally related protein, phosphatidyinositol transfer protein (PITP), colocalized much less well with caveolin-1, was not in close proximity to caveolin-1 (i.e., >120 Å), and was not coimmunoprecipitated by anti-caveolin-1 from cell lysates. In summary, it was shown for the first time that SCP-2 (but not PITP) selectively interacted with caveolin-1, both within the cytoplasm and at the plasma membrane. These data contribute significantly to our understanding of the role of SCP-2 in cholesterol and phosphatidylinositol targeted from intracellular sites of synthesis in the endoplasmic reticulum to caveolae/lipid rafts at the cell surface plasma membrane.

Although the plasma membrane lipid bilayer is a matrix for integrating transport and signaling functions, molecular details of how lipid organization contributes are only now being resolved. Cholesterol, classically thought to function in maintaining optimal membrane fluidity and permeability, is now being recognized as a major force for organizing signaling lipids as well as cell signaling and transport proteins into cholesterol-rich domains termed lipid rafts/caveolae within the plasma membrane (*1*, *2*). While cholesterol is randomly distributed across the plane of the bilayer in model membranes, in plasma membranes (reviewed in refs *3* and *4*) and lipid rafts/caveolae (*5*), cholesterol preferentially distributes into the cytofacial leaflet (i.e., cholesterol-rich) by as yet unresolved mechanisms. In contrast, cholesterol spontaneously distributes into cholesterol-rich (termed lipid rafts) and cholesterol-poor domains in the lateral plane of both model membranes (*1*, *4*) and biological membranes (reviewed in refs *2*−*4* and *6*−*11*). Lipid rafts/caveolae are especially rich in lipids involved in intracellular signaling [phosphatidylinositol (PI), phosphatidylinositol-4-phosphate (PIP), phosphatidylinositol-4,5-bisphosphate (PIP2), ceramide, and diacylglycerol] (*6*, *11*−*14*) and signaling proteins (*11*, *13*). Since disruption of these cholesterol-rich microdomains also inhibits transport and signaling (*13*), it would appear that intact lipid rafts/caveolae are essential for organizing signaling lipids and proteins in close proximity. Because cholesterol and signaling molecule precursors such as PI are synthesized in the endoplasmic reticulum, mechanisms must exist for their preferential transport to plasma membrane caveolae. However, these trafficking pathways are only beginning to be resolved. Sterol carrier protein-2 and caveolin-1 are two proteins involved in the transfer of both cholesterol and phosphatidylinositol.

Cholesterol appears to be transported from intracellular sites to plasma membrane caveolae by both rapid protein-mediated and slow vesicular mechanisms. SCP-2[1] (reviewed in refs *7*, *15*, and *16*) and caveolin-1 (as a complex with chaperone proteins) (*17*, *18*) mediate rapid (half time of 1−2 min) molecular transfer of cholesterol from intracellular sources to plasma membrane caveolae. In contrast, slow (15−20 min) vesicular cholesterol transport occurs via caveolar vesicles budding from the Golgi (reviewed in ref *11*) and

† This work was supported in part by the U.S. Public Health Service, National Institutes of Health Grants GM31651 (F.S.) and GM62326 (J.M.B.).

* To whom correspondence should be addressed. Telephone: (979) 862-1433. Fax: (979) 862-4929. E-mail: fschroeder@cvm.tamu.edu.

‡ Department of Physiology and Pharmacology.

§ Department of Pathobiology.

[1] Abbreviations: SCP-2, sterol carrier protein-2; PITP, phosphatidylinositol transfer protein.

10.1021/bi035914n CCC: $27.50
Published on Web 05/21/2004

vesicles derived from the LDL−receptor−lysosomal endocytic pathway (reviewed in ref *19*). Despite the important role of both SCP-2 and caveolin-1 in cholesterol transfer to plasma membrane caveolae, it is not known whether these proteins directly interact for mediating cholesterol traffic to plasma membrane caveolae.

Phosphatidylinositol transport from its site of synthesis, the endoplasmic reticulum, to plasma membrane caveolae has also been proposed to occur by both protein-mediated molecular transfer and vesicular transfer via caveolin-1 containing vesicles originating from the golgi (reviewed in refs *20*−*22*). SCP-2 (*23*) and another protein, phosphatidylinositol transfer protein (PITP) (*20*, *21*, *24*), enhance rapid PI transfer from the endoplasmic reticulum. However, it is unclear whether these proteins directly interact with caveolin-1 and caveolae at the plasma membrane. For example, immunolocalization of fixed cells detects highest levels of PITPα within nuclei and perinuclear golgi, while PITPβ is primarily distributed to perinuclear golgi (*20*, *25*). Furthermore, neither PITPα nor PITPβ is detected at the plasma membrane (*20*, *25*). The latter observation is puzzling especially in view of the fact that PITP is thought to directly present bound substrate to phospholipase C and to interact with phosphoinositide kinase signaling complex at the plasma membrane caveolae (reviewed in refs *20* and *25*). Subcellular fractionation and immunolocalization reveal that nearly half of total SCP-2 is extraperoxisomal in cytoplasm and/or associated with endoplasmic reticulum or mitochondria (reviewed in refs *15* and *16*). In contrast, immunolabeling confocal microscopy detects some SCP-2 at the plasma membrane (*23*), and SCP-2 overexpression enhances the rapid diffusion of ligands (*16*, *26*), suggesting that SCP-2 participates in molecular PI transfer between intracellular sites and plasma membrane caveolae. Because the limit of resolution of light microscopy is about 2200 Å, it remains to be determined whether these observations reflect direct association of SCP-2 with caveolin-1.

The purpose of the present investigation was to begin to resolve these issues to determine: (i) whether SCP-2 and PITP at the plasma membrane are colocalized with caveolin, (ii) if SCP-2 coimmunoprecipitates with caveolin from cell lysates, (iii) if SCP-2 is associated with purified plasma membranes and lipid rafts/caveolae isolated therefrom, (iv) whether SCP-2 and caveolin are detectable in close proximity as shown by fluorescence resonance energy transfer (FRET) and immunogold electron microscopy of intact cells, and (v) if SCP-2 and caveolin interact directly in a yeast two-hybrid assay. These studies should contribute significantly to our understanding of how SCP-2 participates in intracellular cholesterol trafficking and/or PI trafficking.

MATERIALS AND METHODS

Cells and Media. SCP-2 overexpressing and mock-transfected L-cell fibroblasts (*27*, *28*) were cultured in Higuchi media supplemented with 10% FBS (Hyclone, Logan, UT) and 1 × penicillin and streptomycin (Sigma, St. Louis, MO). SCP-2 overexpressing (*28*) and mock-transfected McA-RH7777 hepatoma cells (*29*) were cultured in DMEM (Gibson, Grand Island, NY) as described (*28*). These cell lines were chosen for several reasons. Thus, fibroblasts represent peripheral cells from which cholesterol effluxes readily (i.e., generally having high levels of caveolin-1, PITP, and low levels of SCP-2). As expected, control (mock-transfected) L-cells have very low SCP-2 levels (about 0.008% of total cytosolic protein) and readily detectable caveolin-1 (*23*, *30*) and PITP (*23*). In SCP-2 overexpressing L-cells, the SCP-2 level was increased 4.3-fold to 0.036% of total cytosolic proteins (reviewed in refs *27* and *31*). Overexpression of SCP-2 results in 4-fold up-regulation of caveolin-1 (*23*). Second, hepatoma cells are derived from liver, a tissue normally containing high levels of SCP-2, PITP, and very little caveolin-1 (*16*). While SCP-2 levels in mock-transfected McA-RH7777 hepatoma cells are about 20-fold lower than in liver, in SCP-2 overexpressing McA-RH7777 hepatoma cells SCP-2 levels were similar to those in liver as detected with Western blot analysis (*29*). Overexpression of SCP-2 in McA-RH7777 hepatoma cells did not alter the level of caveolin-1.

Antibodies. Primary antibodies for imaging and Western blot assay were as follows: anti-SCP-2 was produced in rats or rabbit in our own lab following the protocols described earlier (reviewed in refs *27*, *28*, *31*, and *32*). Mouse monoclonal anti-PITP, mouse monoclonal anti-caveolin-1 rabbit anti-caveolin-1 polyclonal antibody, and anti-flotillin polyclonal antibody were purchased from Transduction Laboratories (BD Biosciences-Transduction Lab, San Diego, CA).

Rat anti-caveolin-1 antiserum was obtained against a 30-residue synthetic peptide corresponding to the N-terminal region of caveolin-1 (Ser-Gly-Gly-Lys-Tyr-Val-Asp-Ser-Glu-Gly-His-Leu-Tyr-Thr-Val-Pro-Ile-Arg-Glu -Gln-Gly-Asn-Ile-Tyr-Lys-Pro-Asn-Asn-Lys-Ala). This peptide [SGGKYVD-SEGHLYTVPIREQGNIYKPNNKA] was prepared by solid-phase peptide chemistry, HPLC purified, and characterized by mass spectroscopy following standard laboratory protocols (*33*, *34*). The full-length peptide product was cross-linked to keyhole limpet hemocyanin (KLH, Sigma Chemical Co., St. Louis, MO) at a ratio of 100 nmol peptide/1 nmol KLH, emulsified in Freund's adjuvant (Pierce, Rockford, IL), and administered by the intramuscular, intraperitoneal, and subcutaneous routes in Sprague Dawley female rats (Harlan, Indianapolis, IN). The peptide specificity of the antiserum was confirmed by ELISA and Western blot analyses.

Rabbit anti-PMP70 was purchased from Zymed (San Francisco, CA), while sheep anti-bovine catalase was from Biodesigns (Saco, Maine). Rabbit anti-Na^+ K^+-ATPase and anti-SR-B1 were purchased from Novus Biologicals (Littleton, CO). Secondary antibodies for imaging were as follows: goat-anti-rabbit-IgG-Rhodamine Red X, anti-mouse-IgG-FITC, and anti-mouse IgG-Texas Red were purchased from Jackson Immunochemistry Laboratories (West Grove, PA). Goat-anti-rat-IgG-FITC was purchased from Sigma (St. Louis, MO), while donkey anti-sheep IgG-Alexa568 was from Molecular Probes (Eugene, OR). Secondary antibodies for immuno-blotting assay were as follows: three alkaline phosphatase conjugates, goat anti-mouse-IgG, anti-rat-IgG and anti-rabbit-IgG, were also purchased from Sigma (St., Louis, MO).

Immunolabeling of Cultured Cells for Laser Scanning Confocal Microscopy. Mock-transfected control and SCP-2 overexpressing hepatoma or L-cells were seeded into four well-chambered coverglasses (Nunc, Fisher Scientific, Pittsburgh, PA) and cultured to approximately 80% confluency

in complete Higuchi media. Cells were washed and fixed in cold methanol/acetone (1:1) as described earlier (*48*). Rat anti-SCP-2, rabbit anti-PMP70, and donkey anti-bovine catalase were diluted at 1:50 in PBS, while mouse anti-caveolin-1 and PITP were diluted at 1:100. A 200 μL aliquot of diluted primary antibodies was added to each well and incubated at room temperature for 1 h. After five washes with PBST (PBS, pH, 7.4, 0.05% Tween-20), secondary antibodies (1:100) were added into each well and incubated for 1 h at room temperature followed by five washes with PBS (pH 7.4). Control staining was done with normal rabbit and mouse sera or by omitting the primary antibodies and using either or both secondary antibodies. This allowed optimization of the concentration of secondary antibodies and hence minimized the nonspecific secondary antibody staining.

Laser Scanning Confocal Microscopy (LSCM). LSCM was performed with a MRC-1024 point scanning laser confocal microscopy system (Bio-Rad, Hercules, CA) equipped with a Zeiss Axiovert 135 inverted microscope, fitted with 63 ×, 1.4 N.A. oil immersion lens (*23*, *28*, *31*, *35*, *36*). FITC was excited with a 15 mW Kr−Ar laser using the 488 nm band, and the emission was detected through a 522/ DF35 filter. Rhodamine Red X, Texas Red, and Alexa568 were excited at the 568 nm band of the Kr−Ar laser, and their emission was detected through a HQ598/40 filter. Confocal images were acquired with Laser Sharp Software (Bio-Rad) and analyzed with Laser Sharp (Bio-Rad), Metamorph (Universal Imaging, the Imaging Division of ASI, Nikon In., Melville, NY), and Adobe Photoshop (Adobe System Inc., Seattle, WA) softwares as described earlier (*23*, *28*, *31*, *35*, *36*). Images were acquired and analyzed using LaserSharp (from Bio-Rad) and MetaMorph Image Analysis (from Advanced Scientific Imaging, Meraux, LA) softwares. Analysis of SCP-2 colocalization with caveolin at the plasma membrane was performed on an average of 20 cells from four different wells, and the results obtained were shown for a representative set of cells. LaserSharp version 3.0 software was used for colocalization analysis and two values (colocalization coefficients) were calculated based on Pearson's correlation coefficient, which is a well-established means of describing the degree of overlap between patterns or images (*37*). The software calculated the colocalization coefficients for two different fluorophores, designated red and green herein, according to the following equations: $C_{red} = \Sigma R_{i,coloc}/\Sigma R_i$ and $C_{green} = \Sigma G_{i,coloc}/\Sigma G_i$. In these equations, $\Sigma R_{i,coloc}$ represents the sum of intensities of all red pixels, which also have a green component; ΣR_i is the sum of all the red pixels in the image; $\Sigma G_{i,coloc}$ represents the sum of intensities of all green pixels that have a red component; and ΣG_i is the sum of intensities of all green pixels in the image. The coefficients generated by LaserSharp have values between 0 and 1; a value of 0 indicates that there is no colocalization, while a value of 1.0 means there is complete colocalization.

Fluorescence Resonance Energy Transfer (FRET) Microscopy. FluorLink-AB Cy3 and Cy5 labeling Kits were purchased from Amersham Pharmacia Biotech Inc. (Piscataway, NJ). Rabbit anti-SCP-2-Cy3/Cy5, mouse anti-caveolin-1 IgG-Cy5, and mouse anti-PITP-Cy3 conjugates were prepared as indicated by the Amersham labeling kit instructions. SCP-2 overexpressing L-cells were cultured in chambered coverglass to about 80% confluency. The cells were washed, fixed, and blocked as described earlier (*23*) followed by incubation in 1:10 diluted Cy3 and Cy5 conjugates for 1 h at room temperature. The cells were washed 5 times in PBS. Fluorescence resonance energy transfer (FRET) was performed with the MRC-1024 LSCM system by the combined acceptor and donor photobleaching methods (pBDIM) (*79*−*81*). Prebleach Cy3 (donor) and Cy5 (acceptor) were excited at 567 and 648 nm, respectively, and emissions were detected through HQ598/40 and 680/30 nm filters, respectively. A sensitized Cy5 image was also obtained upon Cy3 excitation at 567 nm and detection of Cy5 emission through a 680/30 nm filter. To perform FRET, a field of interest was selected and rendered free of Cy5 by bleaching using repeated scanning with the 647 nm laser band at 100% power for 15−20 min. The post-bleached Cy3 and Cy5 images were obtained with the same filter settings as described previously. The FRET efficiencies (E_i) in pixel i in selected cells ($n > 25$) were calculated from image arithmetic of the prephotobleach ($I_{pre,i}$) and postphotobleach ($I_{pst,i}$) Cy3 images (*38*−*40*) according to eq 1.

$$E_i = (I_{pst,i} - I_{pre,i})/I_{pst,i} \quad (1)$$

where E_i was calculated from $n > 20$ cells. The distance between two fluorophores was determined from the energy transfer efficiency E_i, which is related to the distance r separating a given donor and acceptor pair according to eq 2.

$$E_i = 1/[1 + (r/R_o)^6] \quad (2)$$

where R_o is the distance for 50% energy transfer efficiency. For the Cy3 donor and Cy5 acceptor pair, R_o is 50 Å (*38*). When the distance between donor and acceptor is larger than $2 \times R_o$, no FRET occurs (*41*). Since Cy3 and Cy5 labeling and purification of antibodies according to the manufacturer's directions yielded diluted Cy3- and Cy5-tagged antibodies, a range of dilutions was tested for the Cy3- and Cy5-labeled antibodies. A 1:10−1:20 dilution of the Cy3- and Cy5-labeled antibodies was optimal for minimizing nonspecific staining and maximizing the fluorescent signals. Normal rabbit and mouse sera were also included in the blocking buffer to ensure the specificity of staining. Control experiments for cross-talk were performed by recording donor (Cy3) only slide, acceptor (Cy5) only slide, and slide with both donor and acceptor.

Immunoelectron Microscopy. LR White resin, Lowicryl HM20 resin, and gold-labeled polyclonal antibodies against rabbit IgG and rat IgG (Aurion, Wageningen, The Netherlands), were purchased through Electron Microscopy Sciences (Fort Washington, PA). Transfected L-cell fibroblasts and T7 hepatoma cells overexpressing SCP-2 were cultivated on poly-l-lysine coated glass slides and fixed in 4% formaldehyde, 0.1% glutaraldehyde in 0.1 M sodium phosphate buffer, pH 7.4, for 4 h at 4 °C. The cells were stained at 24 °C with 0.5% uranyl acetate in 70% ethanol for 30 min, dehydrated in a graded ethanol series, and then embedded in LR White acrylic resin at 48 °C for 2 days. L-cells and T7 hepatoma cells also were prepared for immunolocalization by low-temperature embedment at −35 °C in Lowicryl HM20 with polymerization by UV light. Ultrathin tissue sections (70−90 nm) were placed on Formvar-coated nickel grids and immunogold stained with

anti-SCP2 antiserum raised in rabbit (diluted 1:25−1:40) alone or in a mixture with anti-caveolin antiserum raised in rat (diluted 1:40). These sections were washed and incubated with a mixture of goat anti-rabbit IgG conjugated to 15 nm gold particles and goat anti-rat IgG conjugated to 6 nm gold particles. Control incubations were also performed without primary antibodies.

Immunoprecipitation and Western Blot Analysis. SCP-2 overexpressing L-cells were cultured in five 75 cm^2 tissue flasks to confluence. The cells were washed with cold PBS (pH 7.4) three times followed by incubation for 10 min on ice in 1 mL/flask of single-detergent lysis buffer (*42*). The lysates were transferred into 1.5 mL tubes, and cell debris was pelleted down at 1000*g* for 5 min. The immunoprecipitation is performed following the procedure described by ref *42*. The cell lysates were precleared with normal rabbit serum to reduce the nonspecific formation of the target proteins−IgG−protein-A−sepharose beads (Sigma, St, Louis, MO). The supernatants were then transferred into fresh tubes followed by immunoprecipitation with rabbit anti-SCP-2 or rabbit anti-caveolin-1 polyclonal antibodies. The immunoprecipitated protein−antibody complexes were removed from protein-A beads by adding 50 μL of 1 × SDS sample buffer and heating at 100 °C for 5 min. After centrifugation at 12 000*g* for 20 s, the samples were loaded onto SDS-15% polyacrylamide gel for resolution. The proteins were then transferred to nitrocellulose membranes in 1 × transfer buffer (*42*). The nitrocellulose membranes were then blocked in 2% BSA-PBST (PBS, pH 7.0, 0.05% Tween-20) overnight at 4 °C, followed by incubating in 1:1000 diluted mouse anti-caveolin-1 monoclonal antibody or 1:1000 diluted rat anti-SCP-2 polyclonal antibody for 2 h at room temperature. The membranes were then washed 5 times with PBST and then incubated in 1:5000 diluted goat-anti-rat-IgG or goat anti-mouse-IgG alkaline phosphatase conjugates for another 2 h. The membranes were washed 5 times in PBS and developed in BCIP/NBT (Sigma, St. Louis, MO).

Biochemical Fractionation of L-Cells Overexpressing SCP-2: Plasma Membranes, Caveolae/Lipid Raft Domains, and Nonraft Domains. A two-step procedure was used to biochemically fractionate SCP-2 overexpressing L-cells to obtain (i) plasma membranes isolated without the use of detergents (*30*, *43*) and (ii) lipid rafts/caveolae and nonraft domains isolated from the purified plasma membranes by concanavalin-A (con-A) sepharose 4B affinity chromatography (*6*). Cells were cultured grown on 12 culture trays (200 × 200 mm, Nalge-Nunc, Milwaukee, WI) for 96 h, washed with PBS, and cultured overnight in serum-free medium. Cells were then rinsed 2 × with PBS, scraped into PBS with protease inhibitor (0.2 μM PMS−F), and sedimented for 5 min at 1000*g*, and the resultant cell pellet was resuspended in buffer A (0.25 M sucrose/5 mM TRIS−HCL, pH 7.8). Cells were then homogenized in a N_2 Bomb Cell Disrupter (Parr Instrument Co., Moline, IL) with 40 psi of N_2 for 13 min. After sedimentation at 1000*g* for 10 min, the postnuclear supernatant was collected, placed on top of 30% Percoll in sucrose/TRIS, and centrifuged at 70 000*g* for 30 min in an SW40Ti rotor on a model XL90 ultracentrifuge (Beckman Instruments, Fullerton, CA). The plasma membrane enriched fraction located at the interphase between the Percoll and the sample layer was collected, sonicated briefly (15 s pulse 3 times over 3 min) using a Fisher 550 Sonic Dismembrator (Fisher Scientific, Pittsburgh, PA), and subjected to con-A sepharose affinity chromatography basically as described (*6*, *44*). The nonadherent fractions eluting from the column were designated nonraft fractions. The conA adherent fraction, eluted with 0.5 M α-methylmannoside, was designated the caveolae/lipid raft enriched fractions. These designations were based on marker assays for caveolae/lipid rafts (caveolin-1, flotillin, SR-B1) and nonrafts (Na^+,K^+-ATPase) determined by Western blot analysis (see next). Both nonraft and caveolae/lipid raft fractions were sedimented at 70 000*g* for 15 h, the pellets were resuspended in minimal amount of wash buffer (buffer X with 1 mM EDTA without $MgCl_2$ or $MnCl_2$), and excess Mn^{2+} resulting in formation of a brown precipitate was removed by briefly centrifuging the sample at 10 000 rpm for 2 min. Western blotting to determine the distribution of marker proteins typically found in caveolae/lipid raft [caveolin-1 (*6*, *45*, *46*), flotillin (*47*), or SR-B1 (*6*, *11*)] and nonlipid raft (Na^+,K^+-ATPase) (*6*, *45*) showed that purified plasma membranes were enriched up to 10-fold in these markers, especially flotillin and Na^+,K^+-ATPase, consistent with the previous citations. The conA nonadherent fraction was highly enriched up to 20-fold in the nonlipid raft marker Na^+,K^+-ATPase but highly reduced in caveolae/lipid raft markers (caveolin-1, flotillin, or SR-B1). In contrast, the conA adherent fraction was enriched up to >10-fold in caveolae/lipid raft markers (caveolin-1, flotillin, or SR-B1) and reduced in nonraft marker (Na^+,K^+-ATPase) as compared to the nonadherent fraction and cell homogenate.

Yeast Two-Hybrid Assay. All reagents and basic procedures (*48*−*50*) for the yeast two-hybrid assay were performed exactly as described in Materials and Methods supplied with the instruction kit Proquest Two-Hybrid System with Gateway Technology (Invitrogen, Carlsbad, CA).

Strains, Media, and Microbiological Techniques. Saccharomyces cerevisiae strain MaV203 (*MAT*α, *leu*2−3, 112, *trp*1−901, *his*3Δ200, *ade*2−101, *gal*4Δ, *gal*80Δ, *SPAL10::URA3*, *Gal*1::*lac*Z, *HIS*3$_{UAS\ GAL1}$::*HIS*3*@LYS*2, *can*1^R, *cyh*2^R) was used to test for interactions of caveolin-1 and SCP-2. A panel of MaV103 (MATa) control strains, containing the same genotype as MaV203 expressing a GAL4 DNA binding fusion protein (DB-X) and a GAL4 transcription activating fusion protein (AD-Y) fusion protein with a spectrum of interaction strengths, were patched onto all assay plates (*48*). The plasmid vectors used were pPC97 (*GAL4*-DB, *LEU2*), pPC97-*CYH2*^{S}, and pPC86 (*GAL4*-AD, *TRP1*) (*48*, *49*, *51*). pDBleu was derived from pPC97 (Invitrogen). All plasmid manipulations were performed according to standard protocol for *Escherichia coli* strains DH5α and electroMAX DH10B cells (*48*). Induction of the *HIS3* and *URA3* reporter genes allowed two-hybrid-dependent transcription activation to be monitored by cell growth on plates lacking histidine or uracil, respectively. The induction of the *lacZ* gene was demonstrated qualitatively using the substrate X-gal (5-bromo-4chloro-3-indolyl-β-d-galactopyranoside). This resulted in yeast colonies turning a blue color. Likewise, a quantitative assay using the substrate, CPRG (chlorophenol red β-D galactopyranoside). This resulted in the production of a reddish brown color.

HIS3 encodes the enzyme, imidazole glycerol phosphate dehydratase, that is inhibited in a dose-dependent manner by 3-amino-1,2,4-triazole (3-AT) (*52*). To increase the

sensitivity of the *HIS3* reporter gene, the MaV203 strain expresses a basal level of *HIS3* that can be titered out using increasing concentrations of 3AT to a point at which growth in the absence of histidine is inhibited. Any growth past this concentration indicates that DB-X (the Gal4 DNA binding domain fusion protein) functions as a transcription activator by itself. To ensure that the DB-X fusion protein does not function as a transcription activator, an inhibition of growth on medium lacking histidine (CSM-Leu-Trp-His) with increasing amounts of 3-amino-1,2,4-triazole (3AT) was evaluated. The following levels of 3AT where included with each colony tested: CSM-Leu-Trp-His + 100 mM 3AT, 75 mM 3AT, 50 mM 3AT, 25 mM 3AT, and 12.5 mM 3AT.

Yeast and bacterial strains were propagated using established methods (Invitrogen ProQuest Two-Hybrid System with Gateway Technology manual). The enriched yeast medium YPAD (yeast extract(Difco)/peptone(Difco)/adenine/2% dextrose) and CSM (complete synthetic medium) lacking the appropriate amino acids have been described (*50*).

SCP-2 Clones. The SCP-2 cDNA was excised from the mammalian SCP-2 overexpression plasmid pKJ1ΔF (*27*) using SmaI and XhoI, ligated into the XmnI and XhoI sites of the Gateway System entry clone, pENTR11 (Invitrogen, CA), transformed into DH5α *E. coli*, and grown under kanamycin selection. The new plasmid, pENTR-SCP2, was restriction enzyme digested, sequence verified, and used to subclone SCP-2 into the expression vectors of the Gateway Expression System, pDEST22 (with the activation domain of the transcription factor, Gal4) and pDEST32 (with the binding domain of the transcription factor, Gal4) for expression in the ProQuest Two-Hybrid System with Gateway Technology (Invitrogen). The recombinant plasmids, pDEST22-SCP2 and pDEST32-SCP2, were extracted from *E. coli* using the Wizard Miniprep Kit and restriction enzyme digested with EcoRV, KpnI, and XhoI (Promega) prior to sequence confirmation.

Caveolin-1 Clones. The caveolin-1 gene was amplified from the vector, pCCaveolin-1 (a gift from Dr. R. G. Anderson, Southwestern Medical Center, Dallas, TX). The caveolin-1 PCR product was generated using Pfu DNA polymerase (Stratagene, La Jolla, CA) and the primers *BP-12* (5′-*ATGTCTGGGGGCAAATA*-3′) and *BP13* (5′-*atatctct-gagTTATATTTCTTTCTGCAAG TTGAT-3*′) by introducing a blunt 5′ end and a 3′ XhoI site for cloning. The thermocycle parameters were as follows: 98 °C for 45 s, 97 °C for 45 s, 50 °C for 45 s, 72 °C for 2 min, cycle for 26 times, and 72 °C for 10 min. The PCR product was purified using a Wizard PCR Prep column (Promega, Madison, WI), quantitated on a 0.7% agarose gel, restriction enzyme digested, purified using a Wizard PCR Prep column, and ligated into the XmnI/XhoI sites of the Gateway System entry clone, pENTR11 (Invitrogen). The new plasmid, pENTR−caveolin-1 was restriction enzyme digested, sequence verified, and used to subclone caveolin-1 into the expression vectors of the Gateway Expression System, pDEST22 and pDEST32 as described previously.

Yeast Two-Hybrid Assay. The ProQuest Two-Hybrid System (Invitrogen) was used to identify the potential interactions of SCP-2 and caveolin-1. SCP-2 was fused to the Gal4 activation domain (amino acid 768−881), and caveolin-1 was fused to the Gal4 binding domain (amino acid 1−147) and transformed into *S. cerevisiae* (*53*). Briefly, *S. cerevisiae* MaV203 was grown in YPAD overnight at 30 °C; diluted to an OD_{600} of 0.5, and incubated at 30 °C with shaking to an OD_{600} of 2. The cells were pelleted, washed with dH_2O, resuspended in 1 mL of 100 mM lithium acetate (LiAc), pelleted, and resuspended in 0.4 mL of 100 mM LiAc, and 50 μL aliquots were placed into microcentrifuge tubes. The cells were pelleted, and the following solutions were added in order: 240 μL of 50% PEG (3350 mw); 36 μL of 1 M LiAc, 25 μL of salmon sperm DNA (2 mg/mL); 50 μL of dH_2O; and 100 ng of plasmid DNA.

A series of yeast transformations were performed to determine the efficiency of the transformation protocol and to test the individual plasmid efficiency of transformation (data not shown). Both fusion proteins were independently transformed into *S. cerevisiae* MaV203 to test each clone for self-activation and determine the concentration of 3-amino-1,2,4-triazole (3AT) required to titrate basal HIS3 expression levels. Both fusion proteins were coexpressed in MaV203.

Initially the transformants were grown on CSM-Leu-Trp at 30 °C for 2−5 days to identify colonies containing both the activating and the DNA binding domain fusion proteins (AD-Y and DB-X). Cotransformed yeast was patched onto master plates, CSM-Leu-Trp, along with five different control yeast containing pairs of control plasmids that ranged from very strong to no interacting plasmids at 30 °C for 48−72 h. The colonies were replica-plated onto media selective for the presence and interaction of both plasmids (CSM-Leu-Trp-Ura; CSM-Leu-Trp-His + 3AT [12.5, 25, 50, 75, and 100 mM 3AT]; YPAD plates contain a nitrocellulose filter for β-galactosidase assays; and CSM-Leu-Trp + 0.2% 5FOA) according to the ProQuest Two-Hybrid System with Gateway Technology manual (Invitrogen).

β-Galactosidase Assays. The production of β-galactosidase was detected both qualitatively and quantitatively on colonies grown on nitrocellulose membrane filters on YPAD plates using the substrate X-gal (5-bromo-4chloro-3-indolyl-β-d-galactopyranoside) and in liquid culture using the substrate CPRG (chlorophenol red β-d-galactopyranoside), respectively, as described by the manufacturer (Invitrogen).

Verification of Candidate Clones. The yeast colonies that demonstrated protein−protein interactions with the induction of the *URA3*, *HIS3*, and β-galactosidase genes were grown in liquid CSM-Leu-Trp medium, and the plasmids were extracted as previously described (*94*). The recovered plasmids were electroporated into ElectroMAX DH10B cells according to the manufacturers' protocol (Invitrogen), restriction enzyme digested, and sequence verified (Gene Technology Laboratory, Texas A & M University, College Station, TX).

Yeast Two-Hybrid Western Blot Assays. Yeast protein extracts were prepared using the Zymo Yeast Protein Extraction kit (Zymo Research, Orange, CA) and used in Western blot assays to detect SCP2- and caveolin-1 fusion proteins. In brief, cells were grown in YPAD medium overnight at 30 °C, and 1×10^6 cells were pelleted. Y-Lysis buffer and zymolyase were added to the samples and incubated at 37 °C for 1 h. The cells were then centrifuged at 400*g* for 5 min, and supernatant was removed. The pellet was resuspended into 1 × SDS−PAGE sample buffer, boiled for 10 min, and separated on a 12% SDS−PAGE. Proteins were transferred to nitrocellulose and probed with rabbit polyclonal anti-SCP-2 antibodies (*74*, *76*−*78*). Pri-

mary antibodies were detected with horseradish peroxide (HRP)-conjugated goat anti-rabbit immunoglobulin (IgG) antibody (Pierce, Rockford, IL) followed by addition of the SuperSignal West Pico Chemiluninescent Substrate (Pierce), and bands were visualized using X-OMAT film (Kodak). The same yeast two-hybrid assays were performed with pDEST22-caveolin-1 and pDEST32-SCP2 to verify positive interactions in both directions.

RESULTS

Intracellular Distribution and Colocalization of SCP-2 with Caveolin-1 in Hepatoma Cells and L-Cell Fibroblasts: Immunofluorescence Confocal Microscopy. The intracellular distribution of SCP-2 and caveolin-1 was examined in mock-transfected McA-RH7777 hepatoma and mock-transfected L-cells by immunolocalization and laser scanning confocal microscopy (LCSM). As indicated in the Materials and Methods, these cells were chosen because their relative proportions of SCP-2 and caveolin differ significantly: McA-RH7777 hepatoma cells contain significantly more SCP-2 than L-cells; L-cells contain significantly more caveolin than hepatoma cells. Hepatoma and L-cells were double immunolabeled with anti-sera to SCP-2 and caveolin-1 followed by reaction with secondary antibodies conjugated to Rhodamine Red X and FITC, respectively.

Although SCP-2 was detected primarily in the perinuclear region, in punctuate intracellular structures, and diffusely throughout the cytoplasm of hepatoma cells (Figure 1A Red), a small but significant amount of SCP-2 was visualized at plasma membrane (Figure 1A, arrows). To determine if the plasma membrane associated SCP2 might be more readily visualized in cells containing less SCP-2, this experiment was repeated with mock-transfected L-cells. While the majority of SCP-2 was also detectable in the perinuclear region, in punctuate intracellular structures, and throughout the cytoplasm of L-cells (Figure 1E, red), plasma membrane staining of SCP-2 was more evident in L-cells (Figure 1E, arrows) than in hepatoma cells (Figure 1A, arrows).

While caveolin-1 levels in hepatoma cells were low, nevertheless caveolin-1 was detectable and primarily distributed in the cytoplasm, both diffusely and as punctuate structures (Figure 1B, green). However, a small amount of caveolin-1 was detected at the plasma membrane clearly visible as a ring at the cell surface (Figure 1B, arrows). The relatively caveolin-1-rich L-cells showed much more caveolin-1 staining intensity, especially in the perinuclear region and diffuse punctuate throughout the cytoplasm (Figure 1F). Again, however, caveolin-1 was distinct caveolin staining was observed at the plasma membranes (Figure 1F, arrows).

To visualize colocalization of SCP-2 with caveolin-1 in hepatoma and L-cells, the simultaneously acquired red (SCP-2) and green (caveolin-1) images were superimposed (Figure 1C,G). While these images showed primarily separate (i.e., noncolocalized) SCP-2 (red pixels) and caveolin-1 (green pixels), a significant amount of colocalized SCP-2/caveolin-1 was visible as yellow pixels (Figure 1C,G). To more clearly distinguish and determine the distribution of the colocalized SCP-2/caveolin-1, the most colocalized yellow pixels were displayed separately (Figure 1D,H). In hepatoma cells, the colocalized SCP-2/caveolin-1 (yellow pixels) were distributed primarily in distinct punctuate structures (Figure 1D) but less so at the plasma membrane (Figure 1D, arrows). In contrast, in L-cells the colocalized SCP-2/caveolin-1 was significantly more concentrated at the plasma membrane (Figure 1H, arrows). Quantitative pixel fluorogram analysis within select plasma membrane regions showed that an average of 24.8 ± 13.4% of SCP-2 -pixels were colocalized with 75.6 ± 15.3% of caveolin-1-pixels within the hepatoma cell plasma membrane (Table 1). In L-cell plasma membranes, 86.7 ± 9.9% of SCP-2-pixels were colocalized with 87.6 ± 10.9% of caveolin-1-pixels (Table 1). When SCP-2 was overexpressed in hepatoma or L-cells and intracellular localization was examined as stated previously, again significant amounts of SCP-2 and caveolin-1 were detected at the plasma membrane, and within the plasma membrane, much of the SCP-2 was colocalized with caveolin-1 (data not shown). These data suggest that both the qualitative and the quantitative distribution of SCP-2 and caveolin-1 were cell-type dependent. Plasma membranes of cells containing little SCP-2 but much caveolin-1 (i.e., L-cells) exhibited 3.5-fold

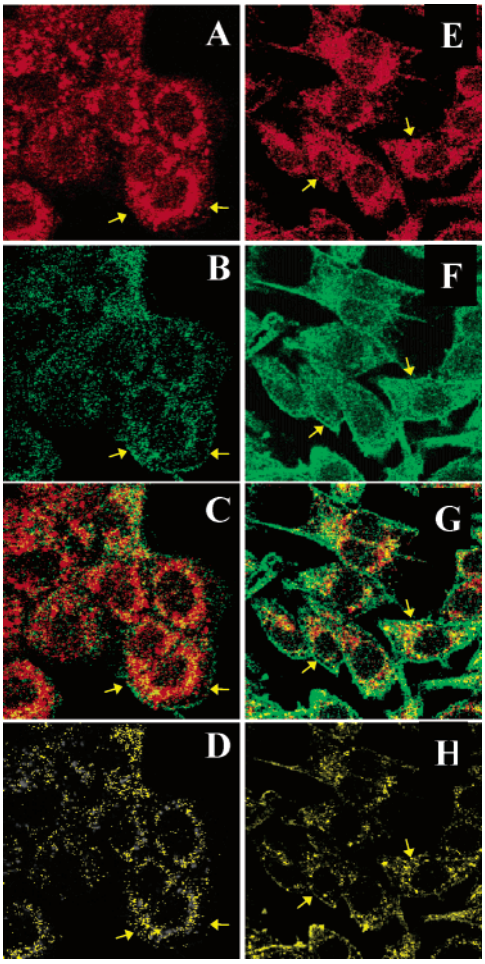

FIGURE 1: Intracellular distribution of SCP-2 and caveolin-1 in hepatoma and L-cells. In fixed cells (hepatoma cells in panels A−D and L-cells in E−H), caveolin-1 was probed with mouse anti-caveolin-1-IgG and goat anti-mouse-IgG-FITC (green), while SCP-2 was probed with rat-anti-SCP-2 and goat anti-rat-IgG- Rhodamine Red X (red). Panels A and E: localization of SCP-2 in hepatoma (A) and L-cells (E). Panels B and F: localization of caveolin-1 in hepatoma (B) and L-cells (F). Panels C and G: overlay of SCP-2 (red) and caveolin (green) images for hepatoma (C) and L-cells (G). Panels D and H: images obtained by selecting the pixels with high fluorescence intensities for both red and green fluorophores in panels C and G, respectively.

Table 1: Colocalization Coefficients for SCP-2, PITP, and Caveolin-1 at the Plasma Membranes of Hepatoma and L-Cells

colocalized proteins (protein1/protein2)	colocalization coefficient (%)[a]			
	hepatoma cells		L-cells	
	protein1	protein2	protein1	protein2
SCP-2/caveolin-1	24.8 ± 13.4	75.6 ± 15.3	86.7 ± 9.9	87.6 ± 10.9
SCP-2/PITP	80.1 ± 13.8	46.6 ± 26.9	86.2 ± 14.8	32.9 ± 19.2
PITP/caveolin-1	72.2 ± 23.0	81.4 ± 11.3	77.3 ± 16.4	86.1 ± 9.0

[a] Regions of interest at the plasma membrane level were selected from 20 cells and LaserSharp version 3.0 software was used for calculation of colocalization coefficients therein as described earlier (*37*) and detailed in Materials and Methods.

more colocalized SCP-2/caveolin-1 than plasma membranes of cells containing high levels of SCP-2 but relatively little caveolin-1 (i.e., hepatoma cells). However, in both cases at least part of SCP-2 was structurally colocalized with caveolin-1, primarily at the plasma membrane in L-cells, and more so in punctate (vesicles) structures containing caveolin-1 in hepatoma cells. While this suggests that perhaps SCP-2 may directly interact with caveolin-1, the limit of resolution of light microscopy (2200 Å) precluded a definitive interpretation.

Determination of Intermolecular Distance between SCP-2 and Caveolin-1 in L-Cells: Fluorescence Resonance Energy Transfer (FRET). While double immunolabeling revealed that in the plasma membrane of both hepatoma and L-cells a high percentage of SCP-2 was colocalized with caveolin-1, the limit of resolution of light microscopy (i.e., 2200 Å) did not permit conclusion of whether SCP-2 interacts/binds directly with caveolin-1. To distinguish this possibility, laser scanning confocal microscopy fluorescence resonance energy transfer (FRET) was performed to determine the intermolecular distance between SCP-2 and caveolin-1 in L-cells. FRET between donor and acceptor fluorescent molecules varies in a highly distance sensitive manner ($1/R^6$) and is dictated by the spectral parameter R_o, the distance at which the FRET efficiency is 50% (*38*−*40*, *54*). Since R_o is characteristic for any given specific donor/acceptor pairs, anti-caveolin-1 and anti-SCP-2 antibodies were conjugated with Cy3 (donor) and Cy5 (acceptor), respectively, as described in Materials and Methods. The Cy3/Cy5 donor/acceptor tags were chosen because (i) these small fluorophores do not significantly alter protein size or charge and (ii) the Cy3/Cy5 pair maximally transfers fluorescence energy when two molecules are <50 Å apart and very weakly transfer energy when two molecules are >72 Å apart (*38*). Efficient FRET is expected to occur from Cy3 to Cy5 only if proteins immunolabeled with these antibody-coupled tags are in very close proximity. The intracellular distributions of Cy3-anti-SCP-2 (donor) (Figure 2A) and Cy5-anti-caveolin-1 (acceptor) (Figure 2C) were basically similar to those detected by primary antibody/tagged-secondary antibody techniques in L-cells (Figure 1). Some differences such as a higher labeling inside nuclei by Cy5-anti-caveolin-1 (Figure 3) than with FITC-anti-IgG-anticaveolin-1 (Figure 1) were due primarily to two factors: (i) differences in quantum yield between the Cy5 and Cy3 (Figure 3) versus FITC and rhodamine red (Figure 1) and (ii) higher laser excitation power and increased detection sensitivity (iris, gain, etc.) required to detect FRET. FRET emission intensities are normally much weaker than emission resulting from direct excitation of the fluorophores. Nevertheless, the overall patterns of SCP-2 and caveolin-1 distribution imaged by Cy3 and Cy5 labeled secondary antibodies were basically similar to those imaged by FITC and rhodamine red secondary antibodies.

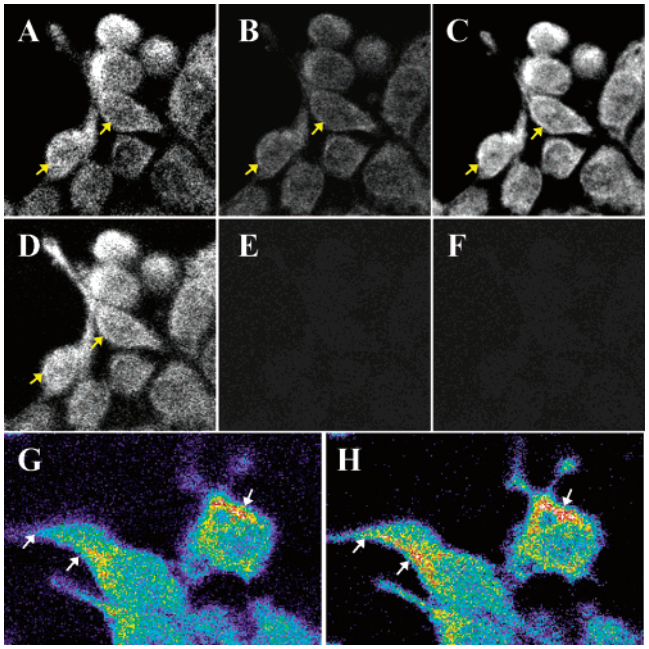

FIGURE 2: Fluorescence resonance energy transfer (FRET) between Cy3-labeled SCP-2 and Cy5-labeled caveolin-1 in L-cells. SCP-2 overexpressing L-cells were fixed and labeled with anti-SCP-2Cy3 and anti-caveolin-1-Cy5 conjugates. FRET was detected as described in the Materials and Methods. Cy3 and Cy5 emission images were detected through HQ590/40 and 680/20 filter, respectively. Panel A: Cy3 (SCP-2) emission acquired with 568 nm band excitation, showing SCP-2 distribution. Panel B: Cy5 (caveolin-1) sensitized emission image detected with Cy3 excitation at 568 nm, indicating energy transfer from Cy3 to Cy5. Panel C: Cy5 emission acquired with direct excitation at 647 nm, showing the caveolin-1 distribution. Panel D: Cy3 emission image acquired with direct excitation at 568 nm after completely bleaching Cy5. Panel E: postbleach Cy5 emission acquired with excitation of Cy3 at 568 nm; no sensitized emission was observed. Panel F: postbleach Cy5 emission acquired with excitation at 647 nm, indicating the total bleaching of the Cy5 fluorescent molecules. Panels G and H: Cy3 fluorescence image with direct excitation of Cy3 at 567 nm, before (G) and after (H) Cy5 photobleach. The images are showed in pseudocolors, which indicate the level of fluorescence intensity on a scale from low (blue and green pixels) through medium (yellow pixels) to high (red pixels) intensity values.

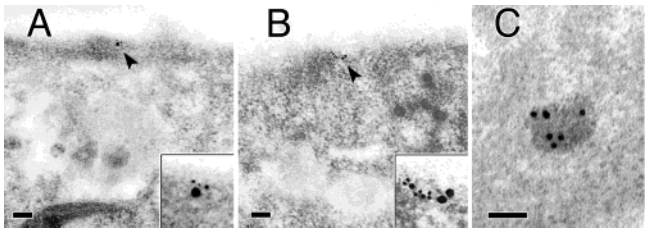

FIGURE 3: Immunogold electron microscopy of SCP-2 and caveolin-1 in L-cells overexpressing SCP-2. Panels A and B are representative images wherein antigenic sites of SCP2 were labeled with 15 nm gold particles and sites of caveolin were labeled with 6 nm gold particles as described in Materials and Methods. Groups of colocalized antigens at the plasma membrane are indicated by arrows and enlarged in the insets. Panel C: antigenic sites of SCP2 were labeled by 15 nm gold particles in peroxisomes of the L-cells. Bar = 100 nm, inset images are enlarged 3×.

First, FRET was observed as the sensitized emission of the acceptor when the donor was excited. Cy3-labeled SCP-2 was excited at 568 nm, and an image of Cy3-labeled SCP-2 emission was acquired through a 590/40 nm band filter (Figure 2A), while simultaneously, the emission of Cy5-labeled caveolin-1 was recorded through a 680/30 nm filter (Figure 2B). Since Cy5 is not excited at 568 nm, this Cy5 image represented FRET-sensitized emission of Cy5 upon Cy3 excitation at 568 nm wavelength. As indicated by the arrows in Figure 2B, caveolin-1 detected by sensitized emission appeared distributed mostly at the plasma membranes of L-cells, clearly indicating that at the plasma membrane the SCP-2 molecules were very close to caveolin-1 (i.e., within less than 100 Å, the limit of FRET sensitivity). By directly exciting Cy-5-anti-caveolin-1 at 647 nm, the fluorescence image of caveolin-1 showed its distribution at the plasma membranes of L-cells but additionally at the peripheral regions of the cytoplasm and even inside nuclei at low extent (Figure 2C).

Second, FRET was observed as an increase in donor emission upon prebleaching the acceptor. Cy5-labeled caveolin-1 emitted strongly when Cy5 was directly excited at 647 nm (Figure 2C), a wavelength at which Cy3 was not excited. The Cy5 fluorescent molecules in the desired field were photobleached by repeat scanning with 647 nm wavelength for 15 min at laser power of 100%. After photobleaching, no Cy5 signal was detected (Figure 2F). The same photobleached area was then excited with 568 nm (Cy3 excitation), and a postbleach Cy3-labeled SCP-2 image was acquired (Figure 2D). The postbleach Cy3 image intensity (Figure 2D) was much stronger than prebleach image intensity especially in the areas indicated by arrows in Figure 2A, consistent with FRET between Cy3-tagged SCP-2 and Cy5-tagged caveolin-1. The increase in donor (Cy3) fluorescence intensity after acceptor (Cy5) photobleach can be easily observed by comparing the images in Figure 2G (prephotobleach) and Figure 2H (postphotobleach): processed images are shown in pseudocolors that indicate the level of fluorescence intensity on a scale from low (blue and green pixels) to medium (yellow pixels) and high (red pixels) intensity values. In Figure 2H (post Cy-5 photobleach), many more yellow and red pixels corresponding to SCP-2 appeared along the plasma membrane (as indicated by arrows). The image pixel intensities of pre- and postbleach Cy3 (obtained through Metamorph software as described in Materials and Methods) were then used to calculate FRET efficiency according to eq 1. The FRET efficiency was as high as 54 $\pm$ 6% ($n = 25$ cells). The intermolecular distance (r) between SCP-2 and caveolin-1, calculated using eq 2, was determined to be 48 $\pm$ 4 Å.

Proximity between SCP-2 and Caveolin-1 at the Plasma Membrane: Immunogold Electron Microscopy. To confirm that SCP-2 detected at the plasma membrane was in close proximity to caveolin-1, L-cells overexpressing SCP-2 were examined by immunogold electron microscopy. The cells were cultured on poly-l-lysine coated glass slides, stained with primary antibodies (i.e., rabbit anti-SCP-2 and rat anti-caveolin-1), stained with secondary antibodies (i.e., goat anti-rabbit IgG conjugated to 15 nm gold particles and goat anti-rat IgG conjugated to 6 nm gold particles), and examined by electron microscopy as described in Materials and Methods. Although the majority of SCP-2 was intracellular, representative electron micrographs showed that both SCP-2 and caveolin-1 were detected in close proximity at the plasma membrane (Figure 3A,B). The intermolecular distance between 15 nm gold particles (detecting SCP-2) and 6 nm gold particles (detecting caveolin-1) determined in six examples from several cells ranged from about 100−240 Å. This range was well within that established for caveolae by morphometric analysis of electon microscrographs, 60−80 nm (*13*, *55*), and by other techniques (*56*−*58*). The rat anti-SCP-2 gold particles closest intermolecular distance (r) between SCP-2 and caveolin-1 was within 100 Å. This distance was somewhat larger than observed by FRET due to (i) repulsive forces between the colloid gold spheres, (ii) the much greater size of the colloidal gold spheres than Cy3 and Cy5 used in FRET, and (iii) the fact that the immunogold measurements were from a much more limited number of sites than represented in the FRET measurements. In summary, the immunogold electron microscopy data indicated that SCP-2 and caveolin-1 were localized in the plasma membrane in regions well within the size of caveolae. Within these plasma membrane regions, some but not all of the SCP-2 was in very close proximity to caveolin-1, thus supporting the FRET measurements.

Specificity of SCP-2 Intracellular Distribution and Colocalization with Caveolin-1 as Compared to that of Another PI Transport Protein: Phosphatidylinositol Transfer Protein (PITP). To determine the specificity of SCP-2 colocalization with caveolin-1, the distribution of PITP, another protein that also binds and transfers PI (*24*, *48*, *59*, *60*), was examined. Since the two isoforms of PITP differently distribute in some cell lines (*62*) and to ensure the specificity of the antigen−antibody reaction, a commercially available monoclonal anti-PITP antibody was used for immunolabeling. This anti-PITP antibody immunoreacted with both PITPα and PITPβ (*23*). While PITP was localized mainly throughout the cytoplasm (Figure 4A,E), small amounts of PITP were detectable at the plasma membranes in both hepatoma (Figure 4A, arrows) and L-cells (Figure 4E, arrows). Although only rarely did PITP pixels appear inside nuclei of either cell line, PITP was most intensely labeled in the perinuclear region and throughout the cytoplasm. Caveolin-1 was localized primarily in the cytoplasm (Figure 4B) and less so at the plasma membrane of hepatoma cells (Figure 4B, arrows). In contrast, in L-cells caveolin-1 appeared much more at the plasma membranes (Figure 4F, arrows). The overlay of green (PITP) and red (caveolin-1) images showed codistribution of the two proteins primarily around nuclei and in the cytoplasm of hepatoma cells (Figure 4C) but most intensely at the plasma membranes of L-cells (Figure 4G, arrows). This pattern of intracellular colocalization was better visualized when only colocalized PITP and caveolin-1 were shown (Figure 4D,H). Quantitative analysis of pixel fluorograms of select plasma membrane regions from multiple cells showed that about 72.2 $\pm$ 23.0 and 77.3 $\pm$ 16.4% of PITP (green) pixels were colocalized with 81.4 $\pm$ 11.2 and 86.1 $\pm$ 9.0% of the caveolin-1 (red) pixels in plasma membranes of hepatoma and L-cells, respectively (Table 1). In hepatoma cell plasma membranes, 2.9-fold more PITP pixels overlapped with caveolin-1 as compared to SCP-2 colocalizing with caveolin-1. In L-cell plasma membranes, a comparable fraction of PITP and SCP-2 (77.3 and 86.7%, respectively) overlapped with

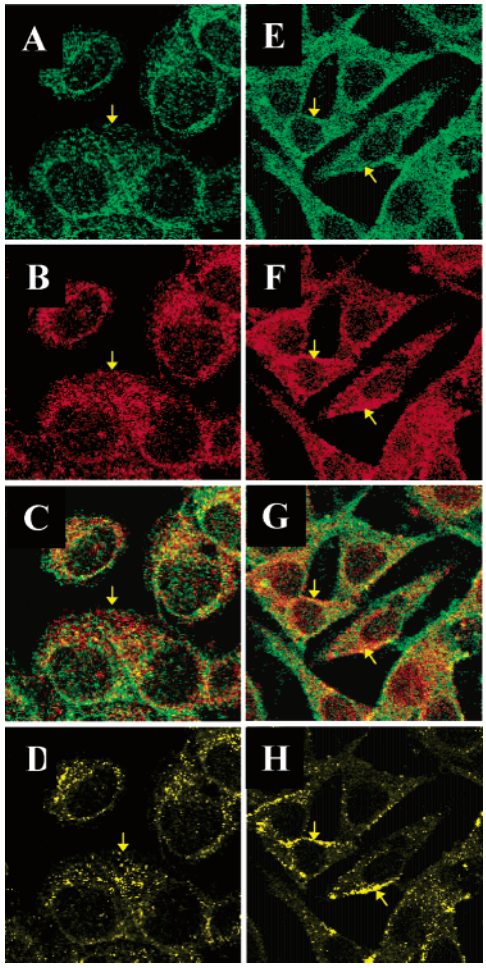

FIGURE 4: Colocalization of PITP and caveolin-1 in hepatoma and L-cells. PITP was probed with mouse anti-PITP and goat anti-mouse-IgG-FITC (green), while caveolin-1 was probed with polyclonal rabbit anti-caveolin-1 and goat anti-rabbit-IgG-Rhodamine Red X (red) in hepatoma (panels A−D) and L-cells (panels E−H). Panels A and E: distribution of PITP in hepatoma (A) and L-cells (E). Panels B and F: localization of caveolin-1 in hepatoma (B) and L-cells (F). Panels C and G: overlay of PITP (green) and caveolin-1 (red) images for hepatoma (C) and L-cells (G). Panels D and H: images obtained by selecting the pixels with highest degree of colocalization (yellow) in panels C and G, respectively.

caveolin-1 (Table 1). In summary, the colocalization of PITP with caveolin-1 appeared to overlap in part with that of SCP-2 with caveolin-1.

Specificity of FRET Analysis for Proximity of SCP-2 to Caveolin-1: Intermolecular Distance between PITP and Caveolin-1. As for FRET between SCP-2 and caveolin-1, the FRET requirement for higher laser excitation power and increased detection sensitivity (iris, gain, etc.) essential to detect FRET also resulted in higher background and somewhat increased intensities of PITP and caveolin in nuclei (Figure 5). Nevertheless, the intracellular distributions of Cy3-anti-PITP (donor) (Figure 5A) and Cy5-anti-caveolin-1 (acceptor) (Figure 5C) were basically similar to those detected by primary antibody/tagged-secondary antibody techniques in L-cells (Figure 2). To determine if FRET occurred from Cy3-labeled PITP (donor) to Cy5-labeled caveolin-1 (acceptor), the possibility of sensitized emission was examined. The Cy3 donor was excited at 568 nm, and an image of Cy3-labeled PITP emission was acquired through a 590/40 nm band filter (Figure 5A), and concomitantly, the emission of Cy5-labeled caveolin-1 was recorded through a 680/30 nm filter (Figure 5B). Since Cy5 is not excited at 568 nm, the Cy5 emits upon FRET from Cy3 (excited at 568 nm) only if caveolin-1 and PITP are in close proximity. Clearly, since Cy5-labeled caveolin-1 sensitized emission was not detectable (Figure 5B); these molecules were not in close proximity. To confirm the lack of significant FRET, Cy3 donor emission was measured upon prebleaching the Cy5 acceptor. Cy5-labeled caveolin-1 emitted strongly when Cy5 was directly excited at 647 nm (Figure 5C), a wavelength at which Cy3 was not excited. The Cy5 fluorescent molecules in the desired field were photobleached by repeat scanning with 647 nm wavelength for 15 min at laser power of 100%. After photobleaching, the Cy5-labeled caveolin-1 was completely bleached (Figure 5E,F). The same photobleached area was then excited with 568 nm (Cy3 excitation), and a postbleach Cy3-labeled PITP image was acquired (Figure 5D). The postbleach Cy3 image intensity (Figure 8D) was very similar to that of the prebleach image intensity (Figure 5A), consistent with weak (if any) FRET between Cy3-tagged PITP and Cy5-tagged caveolin-1. Examination of a large number of cells ($n = 25$) showed that the FRET efficiency between the Cy3-labeled PITP and Cy-5-labeled caveolin-1 was $<0.5\%$, and the distance r was >120 Å. Since the distance r was larger than $2 \times R_o$, this indicated no energy transfer between caveolin-1 and PITP (*38*, *54*).

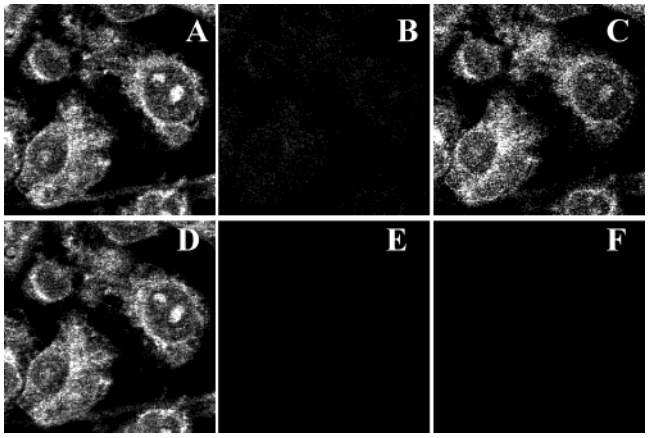

FIGURE 5: Fluorescence resonance energy transfer (FRET) between Cy3-labeled PITP and Cy5-labeled caveolin-1 in L-cells. Cells were probed with anti-caveolin1-Cy5 and anti-PITP-Cy3 conjugates. The donor (Cy3) was excited with 568 nm band and detected through HQ590/40 filter, while the acceptor (Cy5) was excited at 647 nm band and detected through 680/20 filter. Panel A: Cy3 (PITP) emission acquired with 568 nm band excitation, showing PITP distribution. Panel B: Cy5 (caveolin-1) sensitized emission image acquired with excitation of Cy3 at 568 nm, indicating no energy transfer from Cy3(PITP) to Cy5 (caveolin-1). Panel C: Cy5 emission acquired with 647 nm band excitation, showing caveolin-1 distribution. Panel D: Cy3 fluorescence image acquired with 568 nm band excitation after photobleaching Cy5; no increase in fluorescence of Cy3 after Cy5 photobleach was observed. Panel E: postbleach Cy5 emission image with excitation of Cy3 at 568 nm. Panel F: postbleach Cy5 emission with 647 nm band excitation.

Thus, caveolin-1 and PITP did not appear in sufficient proximity for direct interaction. These data, together with the close proximity (48 Å) between SCP-2 and caveolin-1, were consistent with specific direct interaction between SCP-2 and caveolin-1.

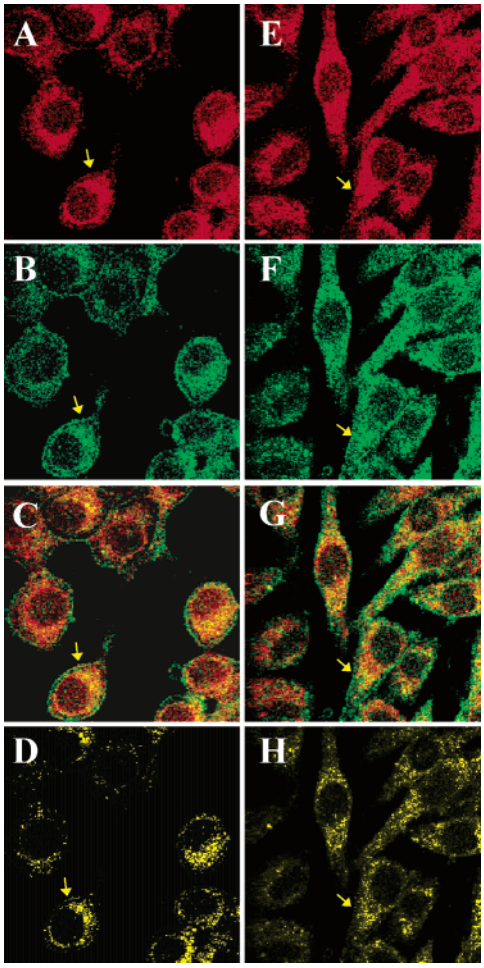

FIGURE 6: Intracellular distribution of SCP-2 and PITP in hepatoma and L-cells. SCP-2 was probed with rabbit anti-SCP-2 polyclonal antibody and goat anti-rabbit-IgG-Rhodamine Red X (red), while PITP was probed with monoclonal mouse-anti-PITP and goat anti-mouse-IgG-FITC (green) in hepatoma (panels A−D) and L-cells (panels E−H). Panels A and E: localization of SCP-2 in hepatoma (A) and L-cells (E). Panels B and F: distribution of PITP in hepatoma (B) and L-cells (F). Panels C and G: overlay of SCP-2 (red) and PITP (green) images for hepatoma (C) and L-cells (G). Panels D and H: images obtained by selecting the pixels with highest colocalization degree (yellow) in panels C and G, respectively.

Confocal Imaging of SCP-2 Codistribution with PITP. Since immunolabeling and confocal microscopy showed that some SCP-2 as well as PITP colocalize with caveolin-1, the possibility that SCP-2 codistributes with PITP was examined. Hepatoma and L-cells were double immunolabeled with anti-SCP-2 and anti-PITP antibodies and examined by confocal microscopy. SCP-2 (red) was localized primarily in the cytoplasm (Figure 6A,E) and less so at the plasma membrane in both hepatoma (Figure 6A, arrows) and L-cells (Figure 6E, arrows). In contrast, PITP (green) was highly distributed in the perinuclear region and throughout the cytoplasm, but significant PITP appeared at the plasma membrane in hepatoma (Figure 6B, arrows) and L-cells (Figure 6F, arrows). Relatively little PITP was detected in nuclei of either cell line. The overlay of red (SCP-2) and green (PITP) images shown for hepatoma cells (Figure 6C) and for L-cells (Figure 6G) demonstrated a high degree of colocalized yellow/orange pixels. After subtracting the background pixels and displaying only colocalized pixels (yellow), the

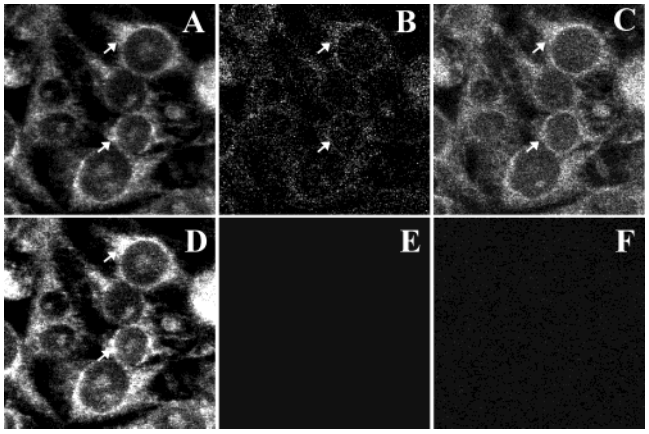

FIGURE 7: Fluorescence resonance energy transfer (FRET) between Cy3-labeled PITP and Cy5-labeled SCP-2 in L-cells. SCP-2 overexpressing L-cells were fixed and probed for SCP-2 with anti-SCP-2-Cy5 and for PITP with anti-PITP-Cy3 conjugates. The donor (Cy3) was excited with 568 nm band and detected through HQ590/40 filter, while the acceptor (Cy5) was excited at 647 nm band and detected through 680/20 filter. Panel A: Cy3 (PITP) emission acquired with 568 nm band excitation, showing PITP distribution. Panel B: Cy5 (SCP-2) sensitized emission image acquired with 568 nm band excitation of Cy3, indicating the energy transfer from Cy3 to Cy5. Panel C: Cy5 emission acquired with 647 nm band excitation, showing SCP-2 distribution. Panel D: postbleach Cy3 emission acquired with 568 nm band excitation. Panel E: Postbleach Cy5 emission with excitation of Cy3 at 568 nm. Panel F: Postbleach Cy5 emission acquired with 647 nm band excitation.

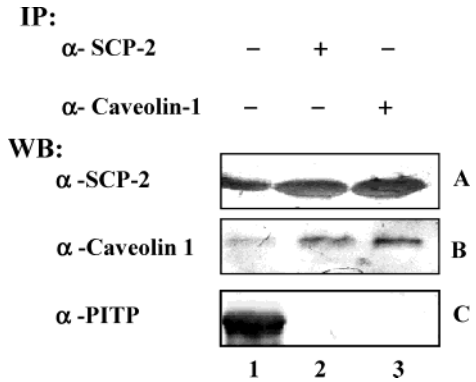

FIGURE 8: Coimmunoprecipitation of SCP-2, caveolin-1, and PITP from SCP-2 overexpressing L-cells. IP, immunoprecipitation of cell lysate was performed with anti-SCP-2 or anti-caveolin-1, as indicated for lanes 2 and 3; WB, Western blots were probed with anti-SCP-2 (A), anti-caveolin-1 (B), and anti-PITP (C). Lane 1: SCP-2 overexpressing L-cell lysate. Lane 2: immunocomplexes precipitated by rabbit anti-SCP-2. Lane 3: immunocomplexes precipitated by mouse anti-caveolin-1.

colocalized SCP-2/PITP appeared primarily in the perinuclear region and punctuate throughout the cytoplasm but much less so at the plasma membranes in hepatoma (Figure 6D) or L-cells (Figure 6H). Quantitative analysis of pixel fluorograms of select plasma membrane areas of multiple cells revealed that the percentage colocalization of SCP-2 with PITP at the plasma membrane level was similar for hepatoma and L-cells. At the plasma membrane a large fraction (i.e., 80.1 ± 13.8 and 86.2 ± 14.8%) of SCP-2-pixels colocalized with a smaller fraction (46.6 ± 26.9 and 32.9 ± 19.4%) of PITP pixels in hepatoma and L-cells, respectively. The fractional number of SCP-2 pixels that colocalized with caveolin-1 was 3.2-fold less than SCP-2 pixels overlapping with PITP in hepatoma plasma mem-

branes (Table 1). In contrast, an equally high percentage of SCP-2 pixels were found colocalized with PITP and with caveolin-1 in L-cell plasma membranes. In summary, these data indicated clearly that SCP-2 was colocalized with PITP primarily in the perinuclear regions, cytoplasm, and somewhat less at the plasma membrane. This colocalization pattern further supported the possibility that both SCP-2 and PITP may contribute to cholesterol transfer and/or PI transfer and PI signaling functions mediated through lipid rafts/caveolae.

Determination of Intermolecular Distance between SCP-2 and PITP in L-Cells: Fluorescence Resonance Energy Transfer (FRET). To further resolve the spatial relationships between SCP-2, caveolin-1, and PITP, the intermolecular distance between SCP-2 and PITP was determined. To show whether FRET occurred from Cy3-labeled PITP (donor) and Cy5-labeled SCP-2, the possibility of sensitized emission was examined. The Cy3 donor was excited at 568 nm, and an image of Cy3-labeled PITP emission was acquired through a 590/40 nm band filter (Figure 7A), and concomitantly, the emission of Cy5-labeled SCP-2 was recorded through a 680/30 nm filter (Figure 7B). Since Cy5 was not excited at 568 nm, the Cy5 emitted upon FRET from Cy3 (excited at 568 nm) only if SCP-2 and PITP were in close proximity. Since Cy5-labeled SCP-2 sensitized emission detected from Cy3-labeled PITP (Figure 7B) was significantly weaker than that of Cy5-lableled caveolin-1 from Cy3-labeled SCP-2 (Figure 7B), this suggested that the SCP-2 was further from PITP than from caveolin-1. To confirm this possibility, Cy3-labeled PITP donor emission was measured upon prebleaching the Cy5-labeled SCP-2 acceptor. Cy5-labeled SCP-2 emitted strongly when Cy5 was directly excited at 647 nm (Figure 7C), a wavelength at which Cy3 was not excited, but not when the Cy5 fluorescent molecules in the desired field were photobleached by repeat scanning with 647 nm wavelength for 15 min at laser power of 100% (Figure 7E). The same photobleached area was then excited at 568 nm (Cy3 excitation), and a postbleach Cy3-labeled caveolin-1 image was acquired (Figure 7D). Although the postbleach Cy3 image intensity (Figure 7D) was higher than that of the prebleach image intensity (Figure 7A), FRET efficiency between the Cy3-labeled PITP and Cy-5-labeled SCP-2 was only $26 \pm 3\%$, and the distance r was 61 ± 2 Å.

Since confocal FRET (i.e., 48 Å) and immunogold electron microscopy showed that SCP-2 (but not PITP) was in close proximity to caveolin-1 at the plasma membrane while FRET microscopy indicated SCP-2 was within 61 Å of PITP, it can be inferred that SCP-2 molecules interacting with PITP were not bound to caveolin-1. Since PITP was sufficiently close to SCP-2 for direct interaction, these data suggest that PITP was localized either (i) more distant from SCP-2 and caveolin-1 within caveolae, (ii) near but not within caveolae, or (iii) near SCP-2 that was not associated with caveolae, caveolar vesicles, or caveolin-chaperone complexes.

Relative Codistribution and Colocalization of SCP-2 with Caveolin-1 as Compared to Peroxisomal Markers: Immunofluorescence Confocal Imaging and Immunogold Electron Microscopy. As indicated previously, SCP-2, PITP, and caveolin-1 were distributed not only at the plasma membrane but also in the cytoplasm often in a punctate pattern. Since previous studies demonstrated that in L-cells about 50% of SCP-2 was associated with peroxisomes, while the rest of SCP-2 was either diffuse in the cytosol or membrane-bound to various organelles (microsomes, mitochondria), the possibility that the punctate distribution of SCP-2 colocalized with caveolin-1 or PITP reflected that of proximity to peroxisomes rather was investigated.

Immunofluorescence confocal imaging and immunogold electron microscopy showed that SCP-2, but not caveolin-1, was highly distributed to peroxisomes. SCP-2 colocalization with catalase, a protein located inside peroxisomes, was analyzed in SCP-2-overexpressing hepatoma cells by confocal microscopy of cells double immunolabeled with antibody against SCP-2 and catalase (see Materials and Methods). Both SCP-2 and catalase were detected as punctuated structures distributed throughout the cytoplasm (data not shown). Quantitative analysis by pixel fluorograms indicated that approximately 45% of SCP-2 was colocalized with 79% of catalase. Similar colocalization percentage was also detected in mock-transfected control hepatoma cells (not shown). These data further supported that a large portion ($\sim$50%) of SCP-2 existed outside the peroxisomes, consistent with tissue fractionation and immunocytochemistry of liver and other tissues (reviewed in ref *16*). SCP-2 overexpressing hepatoma cells were fixed and double immunolabeled with anti-caveolin-1 antibody together with anti-peroxisomal membrane protein-70 (anti-PMP70), found exclusively in peroxisomal membranes. As for catalase, PMP70 was also distributed as punctuate structures throughout the cytoplasm (not shown). In contrast, in the cytoplasm, caveolin-1 was stained much more diffusely and also punctuated structures apparently smaller than peroxisomes. Quantitative analysis of a pixel fluorogram of the superposed images showed that only 28% of caveolin-1 was colocalized with 21% of PMP70. Thus, caveolin-1 colocalized weakly with peroxisomes. Immunogold electron microscopy confirmed that SCP-2, but not caveolin-1, was detected in peroxisomes of SCP-2 overexpressing L-cells as shown by a representative image (Figure 3C).

To examine whether the punctuate distribution of PITP in cytoplasm of hepatoma and L-cells was associated with peroxisomes, cells were double immunolabeled with antibodies against PITP and catalase and analyzed by confocal microscopy. In the cytoplasm of hepatoma cells, both PITP and catalase were detected primarily as separate PITP pixels distinct from catalase pixels (data not shown). Quantitative analysis by a pixel fluorogram indicated that only 23% of PITP was colocalized with 100% of catalase. In cytoplasm of L-cells, PITP and catalase also appeared separately (data not shown). Enhancement and display of only colocalized (yellow) pixels showed that some PITP colocalized with catalase, in catalase-rich regions. This was confirmed by quantitative analysis in the pixel fluorogram that showed only 22% of SCP-2 was colocalized with 74% of catalase. Quantitative pixel fluorogram analysis showed that the colocalization percentage was $\leq$23% in both hepatoma and L-cells. In comparison, 46% of SCP-2 codistributed with catalase in L-cells. These data demonstrated that PITP was much less (i.e., 2-fold) codistributed with peroxisomes as compared to SCP-2.

In summary, immunofluorescence confocal imaging and immunogold electron microscopy indicated that (i) SCP-2 was highly localized in peroxisomes, (ii) caveolin-1 was not detectable in peroxisomes, and (iii) PITP was only weakly colocalized with peroxisomes. These data indicated that SCP-

2, but not caveolin-1, localized in the cytoplasm within peroxisomes. Likewise, PITP also appeared poorly associated with peroxisomes. Thus, intracellular colocalization of SCP-2 with caveolin-1 was not due to caveolin-1 localization near or within peroxisomes.

Coimmunoprecipitation of SCP-2 with Caveolin-1. To confirm the previous FRET data suggesting direct interaction between SCP-2 and caveolin-1, SCP-2 and caveolin-1 were coimmunoprecipitated from L-cells overexpressing SCP-2. When lysates of L-cells overexpressing SCP-2 were individually probed with anti-SCP-2 or anti-caveolin-1 antibodies, it was evident that the L-cells contained much more SCP-2 than caveolin-1 (Figure 8A,B, lane 1). When lysates were immunoprecipitated with anti-SCP-2 or anti-caveolin-antibodies, the immunprecipitates were enriched in SCP-2 (Figure 8A, lane 2) and caveolin-1 (Figure 8B, lane 3), respectively, as compared to the amounts of these proteins present in the lysate (Figure 8A,B, lane 1). Anti-SCP-2 antibody successfully coimmunoprecipitated caveolin-1 (Figure 8B, lane 2) along with SCP-2 (Figure 8A, lane 2). The caveolin-1 band (Figure 8B, lane 2) was severalfold ernriched as compared to caveolin-1 present in the cell lysate (Figure 8B, lane 1). Anti-caveolin-1 antibody successfully precipitated caveolin-1 (Figure 8B, lane 3) and coprecipitated SCP-2 (Figure 8A, lane 3) from homogenates of SCP-2 overexpressing L-cells. The coimmunoprecipitated SCP-2 band (Figure 8A, lane 3) was severalfold more intense than the amount of SCP-2 present in the cell lysate (Figure 8A, lane 1). Likewise, the caveolin-1 band (Figure 8B, lane 3) was severalfold more intense that in the cell lysate (Figure 8B, lane 1). Since both anti-caveolin-1 and anti-SCP-2 coimmunoprecipitated similarly large amounts of SCP-2 but much less caveolin-1, this experiment suggests that a significant amount of SCP-2 interacted with caveolin-1. Thus, SCP-2 and caveolin-1 were coimmunoprecipitated by anti-SCP-2 or anti-caveolin-1 antibodies. These data further supported the possibility that SCP-2 directly interacted with caveolin-1.

Specificity of SCP-2 Coimmunoprecipitation with Caveolin-1. To determine the specificity of SCP-2 coimmunoprecipitation with caveolin-1, coimmunoprecipitation with PITP was examined in homogenates from SCP-2 overexpressing L-cells. Neither anti-SCP-2 nor anti-caveolin-1 antibody coimunnoprecipitated PITP (Figure 8C, lanes 2 and 3, respectively). Since the commercially available monoclonal anti-PITP antibody failed to precipitate PITP under the same precipitation condition used for precipitating caveolin-1 and SCP-2, this precluded direct coimmunoprecipitations with anti-PITP. However, this antibody recognized PITP from Western blots of the cell lysates (Figure 8C, lane 1). In summary, neither anti-SCP-2 nor anti-caveolin-1 coimmunoprecipitated PITP. These data further supported the possibility that the direct interaction of SCP-2 with caveolin-1 was specific.

Cellular Subfractionation to Determine if SCP-2 Distributed to Caveolae/Lipid Rafts Isolated from SCP-2 Overexpressing L-Cells. To determine if SCP-2 was associated with caveolae/lipid rafts purified by subcellular fractionation, plasma membranes were isolated from mock-transfected (control) L-cells and SCP-2 overexpressing L-cells as described in Materials and Methods. The resultant purified plasma membranes were then further subjected to concanavalin-A affinity chromatography to resolve a nonadherent and an adherent fraction. Western blotting with anti-SCP-2 antisera suggested that SCP-2 levels were below the limit of detection in purified plasma membranes from control (mock-transfected) L-cells (Figure 9A, lane 1). However, when these plasma membranes were subfractionated by concanavalin-A affinity chromatography, the caveolae/lipid raft fraction contained detectable SCP-2 (Figure 9A, lane 3), while the nonraft fraction contained no detectable SCP-2 (Figure 9A, lane 2). For SCP-2 overexpressing cells, Western blotting with anti-SCP-2 antisera detected a significant amount of SCP-2 in purified plasma membranes (Figure 9A, lane 4), as well as in the caveolae/lipid raft fraction (Figure 9A, lane 6), but not the nonraft fraction (Figure 9A, lane 5). The amount of SCP-2 detected in the caveolae/lipid raft fraction of SCP-2 overexpressing cells (Figure 9A, lane 6) appeared greater than for control cells (Figure 9A, lane 3). It should be noted that, although the caveolae/lipid raft fraction contained bound SCP-2, the level of SCP-2 was less than in the plasma membrane fraction. This apparent loss of SCP-2 may be due to the fact that SCP-2 is not an integral membrane protein but interacts with the membrane fractions through electrostatic interactions with anionic phospholipids (and/or putative receptor proteins). Because of the volumes involved, SCP-2 was apparently partially lost during the conA affinity chromatography of the plasma membrane fraction to resolve caveolae/lipid rafts from nonraft membrane domains. In summary, SCP-2 was detectable in highly purified plasma membranes isolated by cellular subfractionation. Further resolution of caveolae/lipid rafts from nonraft regions of the plasma membrane revealed that SCP-2 was preferentially localized in caveolae/lipid rafts.

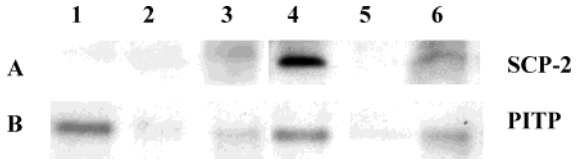

FIGURE 9: Western blotting of SCP-2 and PITP in plasma membranes, caveolae/lipid raft domains, and nonraft domains. Western blotting was performed as described in Materials and Methods. Equal quantities of protein from mock transfected control L-cells (lanes 1−3) and SCP-2 overexpressing L-cells (lanes 4−6) were loaded in each lane: lanes 1 and 4, plasma membrane; lanes 2 and 5, nonraft fraction; and lanes 3 and 6, caveolae/lipid raft fraction. Panel A was detected with anti-SCP-2, while panel B was detected with anti-PITP.

Specificity of SCP-2 Distribution to Caveolae/Lipid Rafts Isolated by Subcellular Fractionation of SCP-2 Overexpressing L-Cells. Western blotting with anti-PITP antisera detected PITP in the plasma membrane fraction of control L-cells (Figure 9B, lane 1). When these plasma membranes were subfractionated by concanavalin-A affinity chromatography, the caveolae/lipid raft fraction contained more PITP (Figure 9B, lane 3) than the nonraft fraction (Figure 9B, lane 2). For SCP-2 overexpressing cells (contain 4-fold more total SCP-2 than controls), Western blotting with anti-PITP antisera detected PITP in plasma membranes (Figure 9B, lane 4) and the caveolae/lipid raft fraction (Figure 9B, lane 6), but it was barely detectable in the nonraft fraction (Figure 9B, lane 5). Again, although the caveolae/lipid raft fraction contained bound PITP, the level of PITP was less than in the plasma membrane fraction. As for SCP-2 in the preceding

section, this may be due to the fact that PITP also interacts with membranes through electrostatic interactions with anionic phospholipids (and/or putative receptor proteins). The losses may be accounted for at least in part to dilutions and conA affinity chromatography of the plasma membrane fraction to resolve caveolae/lipid rafts from nonraft membrane domains. Since PITP was detected in caveolae/lipid rafts, but not coimmunoprecipitated by either anti-SCP-2 or anti-caveolin-1, these data indicate that the PITP most likely was associated with the noncaveolar lipid rafts.

Yeast Two-Hybrid Assay to Determine Interaction between SCP-2 and Caveolin-1 in Vivo: Constructs and Yeast Expression. Since the previous biochemical and immunolabeling approaches were all in vitro methods that were antibody-dependent, these studies were complimented by an in vivo approach that was antibody-independent. The yeast two-hybrid assay was used to determine a protein−protein interaction between SCP2 and caveolin-1 in vivo. All reagents and basic procedures (*48*−*50*) for the yeast two-hybrid assay were performed exactly as described in Materials and Methods. Briefly, SCP-2 cDNA was excised from a mammalian SCP-2 overexpression plasmid and ligated into the entry clone, pENTR11; the recombinant plasmid, pENTR-SCP2 (Figure 10A, right panel) was restriction enzyme digested, sequence verified, and used to subclone SCP-2 into the activating domain fusion (AD-Y) and DNA binding domain fusion (BD-X). SCP-2 was cloned into pDEST22, encoding the activation domain of the Gal4 transcription factor, producing the fusion protein, AD-SCP2 (Figure 10B, bottom left). Likewise, SCP-2 was cloned into pDEST32, encoding the binding domain of the Gal4 transcription factor, producing the fusion protein, BD-SCP2 (Figure 10B, bottom right). Western blot analyses confirmed the expression of the fusion protein for SCP-2 (Figure 11A) in yeast cell lysates. The fusion protein with SCP-2 has a molecular weight of ~30 kDa.

Similarly, the caveolin-1 cDNA was generated and ligated into the entry clone, pENTR11, as described in Materials and Methods. The new plasmid, pENTR-caveolin-1 (Figure 10A, left panel) was restriction enzyme digested, sequence verified, and used to subclone caveolin-1 into pDEST22 producing the Gal4 activating domain-caveolin-1 fusion protein (Figure 10B, top left) and pDEST32 producing the Gal4 DNA binding domain-caveolin-1 fusion protein (Figure 10B, lower right), respectively. Western blot analyses confirmed the expression of the fusion protein for caveolin-1 (Figure 11B) in yeast cell lysates. The fusion protein with caveolin-1 SCP-2 has a molecular weight of ~38 kDa.

Separate yeast two-hybrid experiments were performed using both AD-SCP2 with BD-caveolin-1 and AD-caveolin-1 with BD-SCP2, and both assays were repeated twice. We obtained the same results from all assays.

Yeast Two-Hybrid Assay: Control Strain Growth Patterns. S. cerevisiae strain MaV203 was used to test for interactions of caveolin-1 and SCP-2, and each assay plate contained a panel of MaV103 (MATa) control strains described in Materials and Methods. Growth phenotypes of five yeast control strains produced with the transformation of MaV103 with plasmids encoding DNA binding-fusion proteins and activating domain-fusion proteins demonstrating no interaction (Figure 12A, control A), weak interaction (Figure 12A, control B), moderate interaction (Figure 12A, control C), strong interaction (Figure 12A, control D), and very strong interaction (Figure 12A, control E). Yeast were grown on complete synthetic media (CSM) lacking either leucine (L), tryptophan (T), uracil (U), and/or histidine(H) with 3-amino-1,2,4-triazole (3AT) or 5-fluoroorotic acid (5FOA) as described (Figure 12A). Growth was measured after incubation at for 48 h at 30 °C. Positive interactions were detected by growth on CSM-L-T, CSM-L-T-H + with less than 50 mM 3AT, CSM-L-T-U, and no growth on CSM-L-T + 0.2% 5FOA. In addition, positive interactions were indicated by no growth on CSM-L-T-U but growth on all the other media.

Table 2: CPRG[a] Analyses for β-Galactosidase Activity in Yeast Two-Hybrid Assay

clone	β-gal units[b]
positive control	0.23
negative control	0.09
clone 16 (pD22SCP2 + pD32caveolin-1)	0.280
clone 1 (pD22SCP2 + pD32caveolin-1)	0.202
clone 2 (pD22SCP2 + pD32caveolin-1)	0.240

[a] Chlorophenol red β-D-galactopyranoside (CPRG). [b] β-gal units = 1000 OD570/*t*min volume OD600.

Yeast Two-Hybrid Assay: Growth Patterns of Strains Expressing SCP-2 and Caveolin-1. Growth phenotypes of the strain MaV203 cotransformed with pDEST22-SCP2 (producing the DNA binding fusion protein, DB-SCP2) and pDEST32-caveolin-1 (producing the activating domain fusion protein, AD-caveolin-1) were determined as described in Materials and Methods. Three individual Leu+, Trp+ transformants, clones 1, 2, and 16 were grown on CSM-L-T, CSM-L-T-H + 3AT (12.5, 50, and 100 mM), CSM-L-T-U, and CSM-L-T + 0.2% 5FOA (Figure 12B). Plates were incubated at 30 °C for 48 h and observed for growth. Growth on CSM-L-T, CSM-L-T-H + 3AT with less than 50 mM 3AT, weak to no growth on CSM-L-T-U, and no growth on CSM-L-T + 0.2% 5FOA were considered positive interactions.

Positive SCP-2-caveolin-1 interactions were identified by (i) the induction of the *URA3* gene by weak to no growth on CSM-Leu-Trp-Ura plates and the inhibition of growth on CSM-Leu-Trp + 0.2% 5FOA (Figure 12B). (ii) Induction of the *HIS*3 gene was demonstrated by showing an increased dose-dependent level of inhibition of growth on CSM-Leu, -Trp, and -His + 3AT (Figure 12B). (iii) Induction of the *lacZ* gene was observed in positive yeast colonies turning a blue color when assayed qualitatively on nitrocellulose membranes using X-gal (data not shown) and quantitatively by assaying for β-galactosidase using chlorophenol red β-D-galactopyranoside (CPRG) assay (Table 2). Similar data (not shown) were obtained when SCP-2 and caveolin-1 were fused oppositely to, respectively, the Gal4 DNA binding and activating domains pDEST32-SCP-2 (i.e., BD-SCP-2) and pDEST22-caveolin-1 (i.e., AD-caveolin-1).

In summary, the yeast two-hybrid assay demonstrated a protein−protein interaction between SCP-2 and caveolin-1 in vivo, consistent with the immunocolocalization, FRET, and immunoprecipitation data in the preceding sections.

DISCUSSION

Since both HDL-mediated reverse-cholesterol transport (*11*, *61*) as well as a significant portion of phosphoinositide

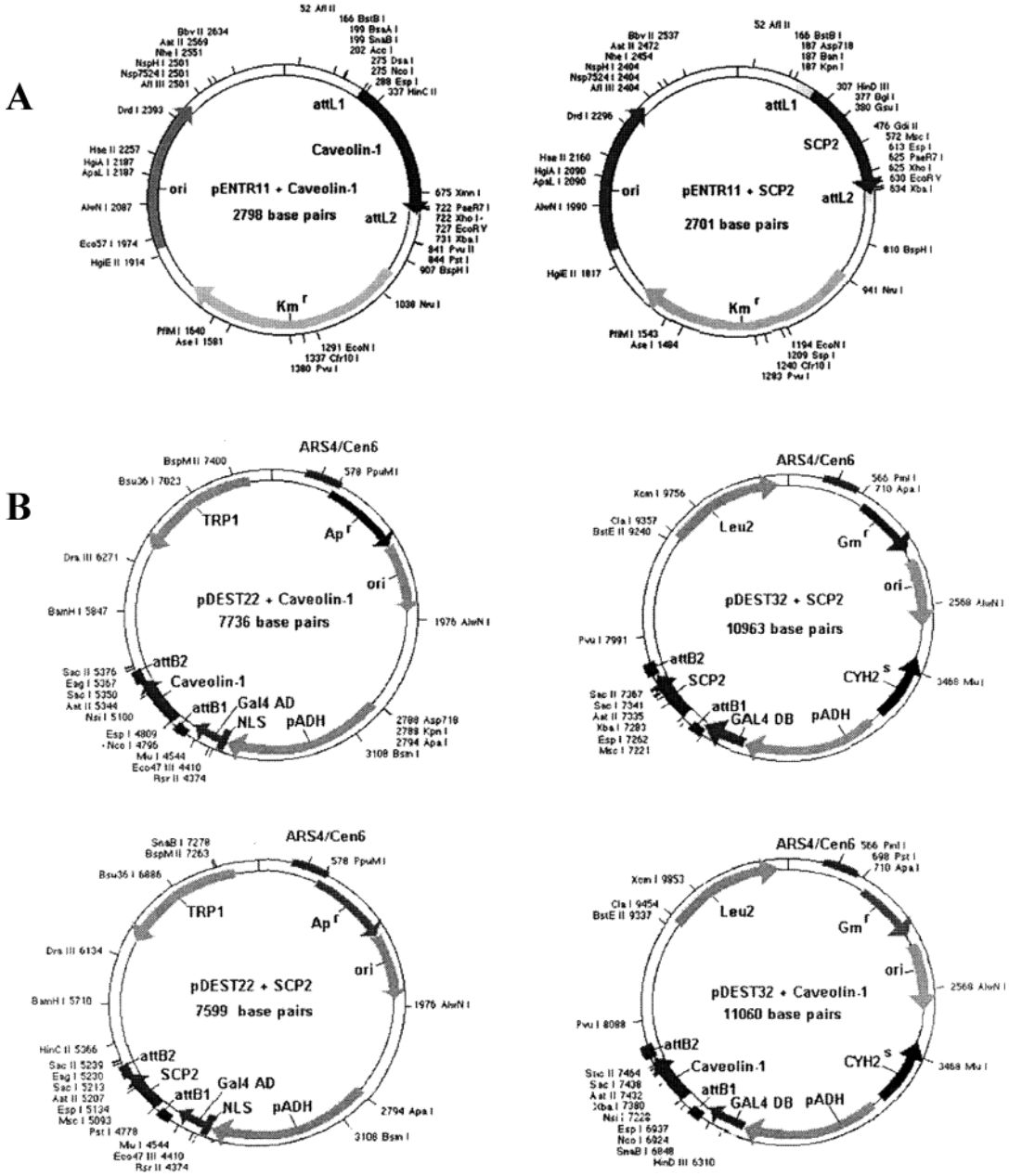

FIGURE 10: Vectors for the yeast two-hybrid assay. Panel A: Gateway entry clones using the shuttle vector, pENTR11, to develop pENTR-SCP2 and pENTR-caveolin-1 were prepared by cloning SCP2 and caveolin-1 genes, respectively, into NcoI and XhoI or XmnI and XhoI restriction enzyme sites. Both inserts are flanked by *att*L1 and *att*L2 recombination sites that are used in a phage λ-based site-specific recombination event to shuttle the SCP2 and caveolin-1 into the Gateway expression vectors. The entry clones contain a pUC origin of replication and the kanamycin resistance gene (Km^r) for maintenance in *E. coli*. Panel B: Gateway DEST clones using the expression vectors, pDEST22 and pDEST32, to use in the ProQuest Yeast Two-Hybrid System (Invitrogen), pDEST22-caveolin-1 (upper left), and pDEST22-SCP2 (lower left) encode fusion proteins containing the transcription activating domain (AD) of the GAL4 transcription factor (generating AD-Y). The pDEST22 clones contain a pUC origin of replication and the ampicillin resistance gene (Ap^r), while the pDEST32 clones encode a gentamycin resistance gene (Gm^r) for maintenance in *E. coli*. The *att*B1 and *att*B2 sites flanking the fusion proteins are the result of *attL* (from pENTR vector) and *attR* (from pDEST vector) site-specific recombination. For expression in yeast, the fusion proteins are under the alcohol dehydrogenase promoter (pADH) with a nuclear localization signal (NLS) and encode for either tryptophan (pDEST22) or leucine (pDEST32) for selection on media without the respective amino acids.

signaling (*2*, *11*, *62*) are mediated through plasma membrane microdomains termed caveolae/lipid rafts, it is important to resolve the mechanism(s) whereby these lipids traffic from intracellular sites of synthesis and are targeted to caveolae/ lipid rafts. Cholesterol transport to caveolae/ lipid rafts occurs by at least two pathways. (i) De novo synthesized cholesterol traffics rapidly (1−2 min) from the endoplasmic reticulum to plasma membrane caveolae/lipid rafts (reviewed in refs *63*−*67*). This rapid cholesterol transport appears mediated by cholesterol binding proteins such as SCP-2 and/or a caveolin-1 complex with cholesterol and chaperone proteins (reviewed in refs *7*, *15*, and *17*). Although SCP-2 is primarily a soluble protein, some SCP-2 has been reported associated with endoplasmic reticulum in fixed cells and in isolated microsomes (reviewed in ref *16*). (ii) Exogenous derived cholesterol (LDL-receptor/lysosomal endocytic pathway) first traffics from lysosomes to the plasma membrane (reviewed in refs *7*, *15*, and *16*) or endoplasmic reticulum (*19*) by rapid protein-mediated transport (e.g., SCP-2) and/or by vesicular transport via the Golgi network (reviewed in refs *7*, *15*, and

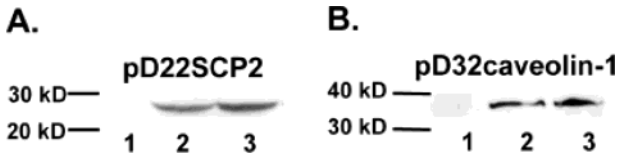

FIGURE 11: Western blot analyses of yeast cell lysates from clones containing pD22SCP2 and pD32caveolin-1. Cell lysates from untransfected MaV203 (lane 1), clone 16 (lane 2), and clone 1 (lane 3) were separated on 12% polyacrylamide (SDS) gels and transferred to nitrocellulose membranes. The blots were probed with (A) rabbit anti-SCP2 antisera or (B) rabbit anti-caveolin-1 antisera and horseradish conjugated-goat anti-rabbit immunoglobulin G. Antibody binding was detected as described in Materials and Methods.

16). Interestingly, both SCP-2 (*16*, *68*) and PITP (*23*) bind long chain fatty acyl CoA (LCFA-CoA), and both SCP-2 (*23*) and PITP (*23*, *59*) bind phosphatidylinositol (PI) and phosphatidylpolyphosphoinositides (poly-PIs). LCFA-CoAs (*69*, *70*) and PIs (reviewed in ref *20*) are potent mediators involved in vesicle budding from the Golgi. PITP is known to stimulate vesicle budding from Golgi (reviewed in ref *20*). Taken together, these data suggest that the intracellular cholesterol binding proteins (SCP-2, caveolin-1) as well as PI binding proteins (SCP-2, PITP) may participate directly or indirectly in cholesterol trafficking from endoplasmic reticulum/Golgi to plasma membrane caveolae/lipid rafts.

Although the previous earlier studies clearly show an involvement of SCP-2 and caveolin-1 in cholesterol trafficking to plasma membrane caveolae/lipid rafts, almost nothing is known regarding mechanism(s) and potential molecular interactions between these proteins in caveolar vesicles and at the target of cholesterol delivery (i.e., caveolae/lipid rafts). To date, only a preliminary report colocalized some SCP-2 with caveolin-1 (*23*). However, the limit of resolution of light microscopy (i.e., 2200 Å) precluded differentiation of whether SCP-2 was actually localized in plasma membrane caveolae and/or caveolar vesicles. The data presented herein make the following new contributions to our understanding of the role of SCP-2 in mediating ligand transfer to plasma membrane caveolae/lipid rafts.

First, double immunolabeling and laser scanning microscopy showed that a significant portion of SCP-2 was colocalized with caveolin-1 (i.e., within 2200 Å), not only in the cytoplasm but also at the plasma membrane of L-cell fibroblasts and hepatoma cells. Within the cytoplasm, the SCP-2 colocalized with caveolin-1 appeared both punctuate and diffuse suggesting that SCP-2/caveolin-1 complexes were membrane-bound and/or diffuse in the cytosol. The punctuate distribution of SCP-2/caveolin-1 codistribution in cytoplasm was distinct from that of SCP-2 and peroxisomes. Although SCP-2 is present in highest concentration in peroxisomes in a punctuate pattern, nearly half of total SCP-2 is extraperoxisomal in L-cells, hepatoma cells, and a variety of tissues (reviewed in ref *16*). Colocalization of SCP-2 with caveolin-1 was significantly greater than colocalization with peroxisomal markers—suggesting SCP-2 colocalization was not just due to caveolar vesicles appearing in the vicinity of peroxisomes within the limit of resolution of optical microscopy (2200 Å). Finally, some of the SCP-2/caveolin-1 colocalized pixels in the cytoplasm also appeared diffuse, consistent with the fact that about 10% of caveolin-1 also exists as a soluble caveolin-1/chaperonin/cholesterol complex in the cytosol (*17*).

Second, cellular subfractionation and immunocoprecipitation studies with SCP-2 overexpressing L-cells and Western blotting further supported the codistribution of SCP-2 and caveolin-1 in plasma membrane caveolae. Western blotting detected SCP-2 in purified plasma membranes, especially in the caveolae/lipid raft as compared to nonraft fraction. Immunoprecipitation studies were consistent with SCP-2 and caveolin-1 interacting in the soluble, cytoplasmic portion of the cell. Anti-SCP-2 and anti-caveolin-1 both coimmunoprecipitated SCP-2 and caveolin-1 from cell lysates of SCP-2 overexpressing L-cells. These data for the first time demonstrated that SCP-2 was not only colocalized with caveolin-1 at the plasma membrane caveolae but also with caveolae/lipid rafts isolated by subcellular fractionation and with caveolin in the cytosol.

Third, fluorescence resonance energy transfer (FRET) distinguished for the first time that SCP-2 was in sufficient proximity for direct interaction with caveolin-1 at the plasma membrane (caveolae) and in the cytoplasm (caveolar vesicles and caveolin/chaperone complexes). FRET detected SCP-2 in close proximity (48 ± 4 Å) to caveolin-1 in L-cells. These data show for the first time that SCP-2 was localized at the plasma membrane and in the cytoplasm in close proximity to caveolin-1 as in plasma membrane caveolae, caveolar vesicles, and/or caveolin-1/ chaperone/cholesterol complexes. Interestingly, SCP-2 overexpression in cultured L-cells inhibits HDL-mediated cholesterol efflux through plasma membrane caveolae mediated by vesicles but accelerates protein-mediated cholesterol transport (*32*). Since the vesicular transport accounts for about 80% of total sterol efflux through caveolae (*32*, *71*), the net effect of SCP-2 was to inhibit sterol efflux. The present data contribute to our understanding of these observations. By directly binding caveolin-1 at the plasma membrane and in cytoplasm, SCP-2 may block the transfer of cholesterol to caveolin-1. Precedent for direct interaction of caveolin-1 with another protein resulting in inhibition of activity is based on studies with endothelial nitric oxide synthase (eNOS). When associated with caveolin-1, the eNOS is inhibited, while uncomplexed eNOS is functionally active (*72*). Thus, although caveolin-1 is very important for organizing signaling molecules and proteins in caveolar structures, direct interaction of caveolin-1 with some proteins (eNOS, SCP-2) results in inhibition of the action of either the interacting protein (eNOS) or caveolin-1.

Fourth, the localization, immunoprecipitation, and proximity of SCP-2 with caveolin-1 were specific. As compared to SCP-2, PITP was less colocalized to caveolin at the plasma membrane, did not colocalize with peroxisomes, did not coimmunoprecipitate with caveolin-1 or SCP-2, and was not in sufficient FRET proximity for direct binding to caveolin-1. Since FRET demonstrated that a fraction of SCP-2 was within 61 ± 2 Å distance of PITP, while PITP was >120 Å away from caveolin-1, this suggested that PITP was near, but could actually be outside, caveolae. This was consistent with the fact that (i) phosphatidylinositol 4-phosphate synthesis occurs both in caveolae and even more so in noncaveolar lipid rafts and (ii) PITP stimulates PI-4-kinase activity in both immunoisolated caveolae and lipid rafts (*14*). The fact that double immunolabeling confocal microscopy colocalized a significant part of SCP-2 and PITP with caveolin-1 at the plasma membrane for the first time provided

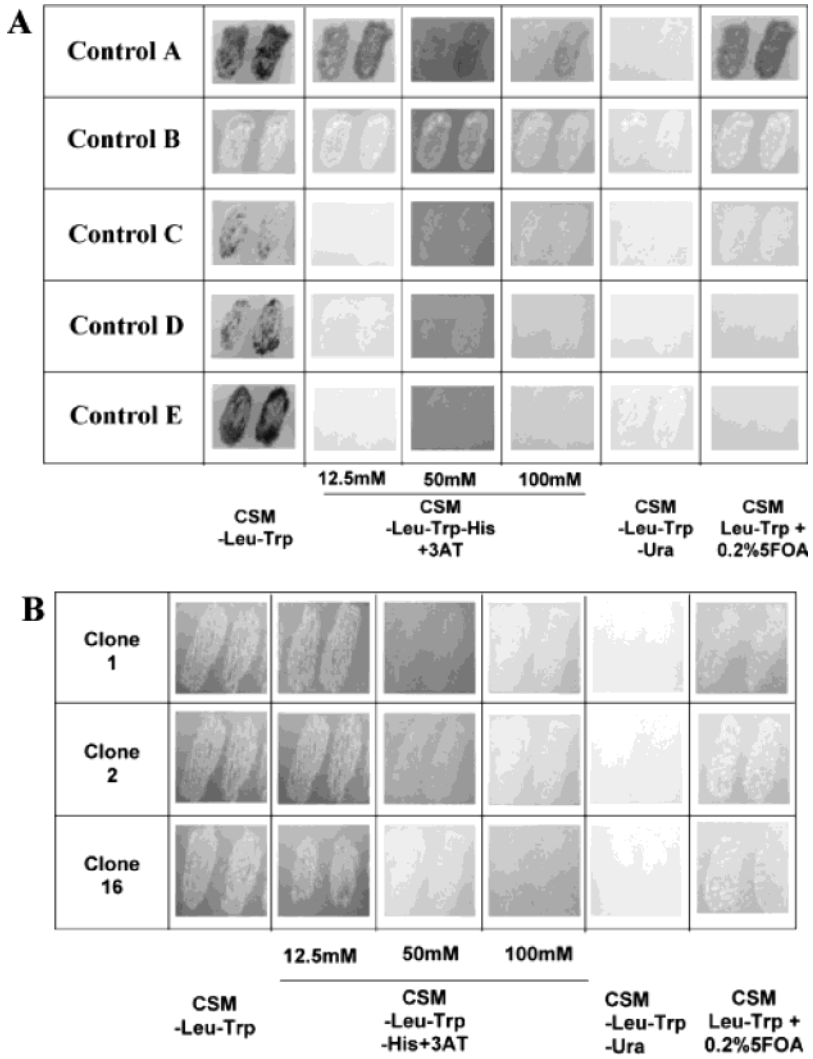

FIGURE 12: Yeast two-hybrid assay examining interaction between caveolin-1 and SCP-2. Panel A: growth phenotypes of five yeast control strains produced with the transformation of MaV103 with plasmids encoding DNA binding-fusion proteins and activating domain-fusion proteins demonstrating no interaction (control A), weak interaction (control B), moderate interaction (control C), strong interaction (control D), and very strong interaction (control E). Patches of cells were grown on complete synthetic media lacking leucine (L), tryptophan (T), uracil (U), and/or histidine(H) with 3-amino-1,2,4-triazole (3AT) or 5-fluoroortic acid (5FOA) [CSM-L-T, CSM-L-T-H + 3AT (12.5, 50, and 100 mM), CSM-L-T-U, and CSM-L-T + 0.2% 5FOA]. The plates were incubated at 30 °C for 48 h and observed for growth. Growth on CSM-L-T, CSM-L-T-H + with less than 50 mM 3AT), CSM-L-T-U, and no growth on CSM-L-T + 0.2% 5FOA were considered positive interactions. No growth on CSM-L-T-U with growth on all the other media was also considered as a positive interaction. Panel B: growth phenotypes of the strain MaV203 cotransformed with pDEST22-SCP2 (DB-SCP2 DNA binding fusion protein) and pDEST32-caveolin-1 (AD-caveolin-1 activating domain fusion protein) were determined. Three individual Leu+; Trp+ transformants; and clones 1, 2, and 16 were grown on CSM-L-T, CSM-L-T-H + 3AT (12.5, 50, and 100 mM), CSM-L-T-U, and CSM-L-T + 0.2% 5FOA. The plates were incubated at 30 °C for 48 h and observed for growth. Growth on CSM-L-T, CSM-L-T-H + 3AT with less than 50 mM 3AT), CSM-L-T-U, and weak to no growth on CSM-L-T + 0.2% 5FOA were considered positive interactions.

ultrastructural evidence consistent with the hypothesis that these proteins also potentially deliver phosphatidylinositol (PI) to signaling complexes (receptors, phospholipase C, PI4 kinase, PI5 kinase) present in caveolae/lipid rafts (reviewed in ref *20*). Finally, while SCP-2 specifically inhibited vesicular transport of cholesterol to plasma membrane (*32*), in contrast, PITIP activates Golgi-vesiculation (reviewed in refs *20* and *73*). Thus, while sharing multiple ligand specificities (PI, LCFA-CoA) and in vitro activities (reviewed in refs *20*, *23*, and *73*), SCP-2 and PITP may exert opposing influences on functions such as cholesterol efflux.

Fifth, in addition to these data obtained in vitro, a yeast two-hybrid assay demonstrated the protein−protein interaction between SCP-2 and caveolin-1 in vivo. The advantages of the ProQuest yeast two-hybrid system with Gateway technology are as follows: (1) that a positive interaction depends on the induction of three independent genes at different loci; (2) it provides four phenotypes [His^+ ($3AT^R$), β-gal, Ura^+, and $5FOA^S$]; and (3) the vectors are low copy plasmids (ARS/CEN6 sequence for replication) to reduce the expression levels and prevent toxicity to the yeast. As detected by growth in culture and galactosidase activity, the yeast two-hybrid assay in both directions showed positive interaction of SCP2 with caveolin-1. Although the interaction detected in the yeast-two hybrid assay was fairly small, nevertheless it was positive.

While the molecular basis for SCP-2 interaction with caveolin-1 remains to be resolved, sequence analysis provides some insights. Caveolin-1 is known to have a scaffolding domain (amino acids 80−101 through which many, but not all, caveolin-1-interacting proteins interact with caveolin-1 (*74*)). Proteins that interact with the caveolin-1 scaffolding

domain contain amino acid sequences of YXYXXXY or YXXXXYXY where Y is aromatic (*74*). Since SCP-2 does not contain either of these types of sequences, it represents a protein that does not have a consensus sequence for interaction with the scaffolding domain of caveolin-1.

The physiological significance of a small portion of total SCP-2 interacting with caveolin-1, especially at the plasma membrane, may be rationalized within the context of the effects of SCP-2 overexpression on functions mediated through caveolae/lipid rafts. For example, SCP-2 overexpression in L-cells dramatically alters the structure, cholesterol, phosphatidylinositol content, and cholesterol dynamics of lipid rafts/caveolae isolated from these cells (*75*, *75*). Furthermore, SCP-2 overexpression reduces HDL-mediated cholesterol efflux through caveolae (*32*) and enhances intracellular cycling of cholesterol (*29*). Caveolin-1 is primarily a membrane structural protein that favors concentration of cholesterol within specific regions of plasma membranes, while SCP-2 is a protein that binds, circulates within the cytosol, and exchanges cholesterol with various membrane bound organelles, down the concentration gradient of cholesterol. These proteins appear to have opposite functions: caveolin-1 accumulates, makes a local pool of cholesterol; SCP-2 equally distributes cholesterol and other membrane lipid components among all the intracellular membranes. Previous work has demonstrated that SCP-2 overexpression in L-cells resulted in inhibition of HDL-mediated cholesterol efflux at caveolar location. The finding that a fraction of SCP-2 is located in the caveolae and physically interacts with caveolin-1 indicates a possible molecular mechanism to explain this physiological effect of SCP-2 in L-cells. How cholesterol is channeled from caveolae to HDL or vice-versa through the SR-BI receptor is poorly understood, and the effect of SCP-2 on this process is still to be studied. A similar inhibitory action has been observed upon eNOS interaction with caveolin-1 (*72*). Finally, SCP-2 interaction with caveolin-1 contributes significantly to our understanding of how phosphatidylinositol may be targeted from intracellular sites of synthesis in the endoplasmic reticulum to caveolae/lipid rafts at the cell surface plasma membrane. The interaction of SCP-2 with caveolin-1 in plasma membrane caveolae may facilitate transfer of bound PI ligand to the phosphatidylinositol 4-kinase signaling complex and thereby contribute to the enhancement of phospholipase C mediated inositol-3-phosphate production in SCP-2 overexpressing cells (*23*). Interestingly, SCP-2 (but not PITP) colocalized within a few angstroms of caveolin-1, and SCP-2 (but not PITP) was coimmunoprecipitated with antisera to caveolin-1 or antisera to SCP-2. This suggests that, although PITP stimulates the phospholipase C signaling complex in plasma membrane caveolae (*23*), the mechanism observed with SCP-2 is distinct.

ACKNOWLEDGMENT

The helpful technical assistance of Ms. Kerstin Krueger was much appreciated.

REFERENCES

1. Bretscher, M. S., and Munro, S. (1993) Cholesterol and the Golgi apparatus, *Science 261*, 1280−1281.
2. Anderson, R. G. W., and Jacobson, K. (2002) A role for lipid shells in targeting proteins to caveolae, rafts, and other lipid domains, *Science 296*, 1821−1825.
3. Schroeder, F., and Nemecz, G. (1990) Transmembrane Cholesterol Distribution, in *Advances in Cholesterol Research* (Esfahami, M., Swaney, J., Eds.) pp 47−87, Telford Press, Caldwell, NJ.
4. Schroeder, F., Frolov, A. A., Murphy, E. J., Atshaves, B. P., Jefferson, J. R., Pu, L., Wood, W. G., Foxworth, W. B., and Kier, A. B. (1996) Recent advances in membrane cholesterol domain dynamics and intracellular cholesterol trafficking, *Proc. Soc. Exp. Biol. Med. 213*, 150−177.
5. Pitto, M., Brunner, J., Ferraretto, A., Ravasi, D., Palestini, P., and Masserini, M. (2000) Use of a photoactivatable GM1 ganglioside analogue to assess lipid distribution in caveolae bilayer, *Glycoconj. J. 17*, 215−222.
6. Atshaves, B. P., Gallegos, A., McIntosh, A. L., Kier, A. B., and Schroeder, F. (2003) Sterol carrier protein-2 selectively alters lipid composition and cholesterol dynamics of caveolae/lipid raft versus nonraft domains in L-cell fibroblast plasma membranes, *Biochemistry 42*, 14583−14598.
7. Schroeder, F., Gallegos, A. M., Atshaves, B. P., Storey, S. M., McIntosh, A., Petrescu, A. D., Huang, H., Starodub, O., Chao, H., Yang, H., Frolov, A., and Kier, A. B. (2001) Recent advances in membrane cholesterol microdomains: rafts, caveolae, and intracellular cholesterol trafficking, *Exp. Biol. Med. 226*, 873−890.
8. Wood, W. G., Rao, A. M., Igbavboa, U., and Semotuk, M. (1993) Cholesterol exchange and lateral cholesterol pools in synaptosomal membranes of pair-fed control and chronic ethanol-treated mice, *Alcohol Clin. Exp. Res. 17*, 345−350.
9. Brown, D. A., and London, E. (2000) Structure and function of sphingolipid- and cholesterol-rich membrane rafts, *J. Biol. Chem. 275*, 17221−17224.
10. Ikonen, E. (2001) Roles of lipid rafts in membrane transport, *Curr. Opin. Cell Biol. 13*, 470−477.
11. Smart, E. J., and van der Westhuyzen, D. R. (1998) Scavenger receptors, caveolae, caveolin, and cholesterol trafficking, in *Intracellular Cholesterol Trafficking* (Chang, T. Y., Freeman, D. A., Eds.) pp 253−272, Kluwer Academic Publishers, Boston.
12. Anderson, R. G. W. (1993) Plasmalemmal caveolae and GPI-anchored membrane proteins, *Cell Biol. 5*, 647−652.
13. Anderson, R. (1998) The caveolae membrane system, *Annu. Rev. Biochem. 67*, 199−225.
14. Waugh, M. G., Lawson, D., Tan, S. K., and Hsuan, J. J. (1998) Phosphatidyl 4-phosphate synthesis in immunoisolated caveolae-like vesicles and low buoyant noncaveolar membranes, *J. Biol. Chem. 273*, 17115−17121.
15. Schroeder, F., Frolov, A., Schoer, J., Gallegos, A., Atshaves, B. P., Stolowich, N. J., Scott, A. I., and Kier, A. B. (1998) Intracellular cholesterol binding proteins, cholesterol transport, and membrane domains, in *Intracellular Cholesterol Trafficking* (Chang, T. Y., Freeman, D. A., Eds.) pp 213−234, Kluwer Academic Publishers, Boston.
16. Gallegos, A. M., Atshaves, B. P., Storey, S. M., Starodub, O., Petrescu, A. D., Huang, H., McIntosh, A., Martin, G., Chao, H., Kier, A. B., and Schroeder, F. (2001) Gene structure, intracellular localization, and functional roles of sterol carrier protein-2, *Prog. Lipid Res. 40*, 498−563.
17. Uittenbogaard, A., Ying, Y. S., and Smart, E. J. (1998) Characterization of a Cytosolic Heat-shock Protein-Caveolin Chaperone Complex, *J. Biol. Chem. 273*, 6525−6532.
18. Smart, E. J., Ying, Y., Donzell, W. C., and Anderson, R. G. W. (1996) A role for caveolin in transport of cholesterol from endoplasmic reticulum to plasma membrane, *J. Biol. Chem. 271*, 29427−29435.
19. Underwood, K. W., Jacobs, N. L., Howley, A., and Liscum, L. (1998) Evidence for a Cholesterol Transport Pathway from Lysosomes to Endoplasmic Reticulum That Is Independent of the Plasma Membrane, *J. Biol. Chem. 273*, 4266−4274.
20. Cockcroft, S. (1999) Mammalian phosphatidylinositol transfer protein: emerging roles in signal transduction and vesicular traffic, *Chem. Phys. Lipids 98*, 23−33.
21. Jones, S. M., Alb, J. G., Jr., Phillips, S. E., Bankaitis, V. A., and Howell, K. E. (1998) A Phosphatidylinositol 3-Kinase and Phosphatidylinositol Transfer Protein Act Synergistically in Formation of Constitutive Transport Vesicles from the Trans-Golgi Network, *J. Biol. Chem. 273*, 10349−10354.

22. Sha, B., and Luo, M. (1999) PI transfer protein: the specific recognition of phospholipids and its functions, *Biochim. Biophys. Acta 1441*, 28−277.
23. Schroeder, F., Zhou, M., Swaggerty, C. L., Atshaves, B. P., Petrescu, A. D., Storey, S., Martin, G. G., Huang, H., Helmkamp, G. M., and Ball, J. M. (2003) Sterol carrier protein-2 functions in phosphatidylinositol transfer and signaling, *Biochemistry 42*, 3189−3202.
24. Borror, C. A., and Helmkamp, G. M. (1991) Transport of phosphatidylinositol to rat hepatocyte plasma membrane catalyzed by phosphatidylinositol transfer protein, *Biochim. Biophys. Acta 1068*, 52−60.
25. De Vries, K. J., Westerman, J., Bastiaens, P. I., Jovin, T. M., Wirtz, K. W. A., and Snoek, G. T. (1996) Fluorescently labeled phosphatidyinositol transfer protein isoforms (a and b), microinjected into fetal bovine heart endothelial cells, are targeted to distinct intracellular sites, *Exp. Cell Res. 227*, 33−39.
26. McArthur, M. J., Atshaves, B. P., Frolov, A., Foxworth, W. D., Kier, A. B., and Schroeder, F. (1999) Cellular uptake and intracellular trafficking of long chain fatty acids, *J. Lipid Res. 40*, 1371−1383.
27. Moncecchi, D. M., Murphy, E. J., Prows, D. R., and Schroeder, F. (1996) Sterol carrier protein-2 expression in mouse L-cell fibroblasts alters cholesterol uptake, *Biochim. Biophys. Acta 1302*, 110−116.
28. Schroeder, F., Frolov, A., Starodub, O., Russell, W., Atshaves, B. P., Petrescu, A. D., Huang, H., Gallegos, A., McIntosh, A., Tahotna, D., Russell, D., Billheimer, J. T., Baum, C. L., and Kier, A. B. (2000) Pro-sterol carrier protein-2: role of the N-terminal presequence in structure, function, and peroxisomal targeting, *J. Biol. Chem. 275*, 25547−25555.
29. Baum, C. L., Reschly, E. J., Gayen, A. K., Groh, M. E., and Schadick, K. (1997) Sterol carrier protein-2 overexpression enhances sterol cycling and inhibits cholesterol ester synthesis and high-density lipoprotein cholesterol secretion, *J. Biol. Chem. 272*, 6490−6498.
30. McIntosh, A., Gallegos, A., Atshaves, B. P., Storey, S., Kannoju, D., and Schroeder, F. (2003) Fluorescence and multiphoton imaging resolve unique structural forms of sterol in membranes of living cells, *J. Biol. Chem. 278*, 6384−6403.
31. Starodub, O., Jolly, C. A., Atshaves, B. P., Roths, J. B., Murphy, E. J., Kier, A. B., and Schroeder, F. (2000) Sterol carrier protein-2 immunolocalization in endoplasmic reticulum and stimulation of phospholipid formation, *Am. J. Physiol. 279*, C1259−C1269.
32. Atshaves, B. P., Starodub, O., McIntosh, A. L., Roths, J. B., Kier, A. B., and Schroeder, F. (2000) Sterol carrier protein-2 alters HDL-mediated cholesterol efflux, *J. Biol. Chem. 275*, 36852−36861.
33. Huang, H., Ball, J. A., Billheimer, J. T., and Schroeder, F. (1999) The sterol carrier protein-2 amino terminus: a membrane interaction domain, *Biochemistry 38*, 13231−13243.
34. Huang, H., Schroeder, F., Zeng, C., Estes, M. K., Schoer, J., and Ball, J. A. (2001) Membrane interactions of a novel viral enterotoxin: rotavirus nonstructural glycoprotein NSP4, *Biochemistry 40*, 4169−4180.
35. Atshaves, B. P., Storey, S., McIntosh, A. L., Petrescu, A. D., Lyuksyutova, O. I., Greenberg, A. S., and Schroeder, F. (2001) Sterol carrier protein-2 expression modulates protein and lipid composition of lipid droplets, *J. Biol. Chem. 276*, 25324−25335.
36. Schoer, J., Gallegos, A., Starodub, O., Petrescu, A., Roths, J. B., Kier, A. B., and Schroeder, F. (2000) Lysosomal membrane cholesterol dynamics: role of sterol carrier protein-2 gene products, *Biochemistry 39*, 7662−7677.
37. Manders, E. M. M., Verbeek, F. J., and Aten, J. A. (1993) Measurement of colocalization of objects in dual-color confocal images, *J. Microsc. 169*, 375−382.
38. Wouters, F., Bastiaens, P. I., Wirtz, K. W., and Jovin, T. M. (1998) FRET microscopy demonstrates molecular association of non-specific lipid transfer protein (nsL-TP) with fatty acid oxidation enzymes, *EMBO J. 17*, 7179−7189.
39. Bastiaens, P. I. (1996) *Proc. Natl. Acad. Sci. 93*, 8407−8412.
40. Bastiaens, P. I. (1998) in *Cell Biology: A Laboratory Handbook* (Celis, J. E., Ed.) pp 136−146, Academic Press, New York.
41. Kenworthy, A. K. (2001) Imaging protein−protein interactions using fluorescence resonance energy transfer microscopy, *Methods 24*, 289−296.
42. Sambrook, J., Fritsch, E. F., and Maniatis, T. (1989) *Molecular Cloning, A Laboratory Manual*, 2nd ed., Cold Spring Harbor Laboratory, Plainview, NY.
43. Gallegos, A. M., Atshaves, B. P., Storey, S., McIntosh, A., Petrescu, A. D., and Schroeder, F. (2001) Sterol carrier protein-2 expression alters plasma membrane lipid distribution and cholesterol dynamics, *Biochemistry 40*, 6493−6506.
44. Schroeder, F., Fontaine, R. N., and Kinden, D. A. (1982) LM fibroblast plasma membrane subfractionation by affinity chromatography on ConA-sepharose, *Biochim. Biophys. Acta 690*, 231−242.
45. Eckert, G. P., Igbavboa, U., Muller, W., and Wood, W. G. (2003) Lipid rafts of purified mouse brain synaptosomes prepared with or without detergent reveal different lipid and protein domains, *Brain Res. 962*, 144−150.
46. Smart, E. J., Ying, Y., Mineo, C., and Anderson, R. G. W. (1995) A detergent-free method for purifying caveolae membrane from tissue culture cells, *Proc. Natl. Acad. Sci. 92*, 10404−10408.
47. Bickel, P. E., Scherer, P. E., Schnitzer, J. E., Oh, P., and Lisanti, M. P. (1997) Flotillin and epidermal surface antigen define a new family of caveolae-associated integral membrane proteins, *J. Biol. Chem. 272*, 13793−13802.
48. Vidal, M. (1997) The reverse two-hybrid system, in *The Two-hybrid System* (Bartel, P., Fields, S., Eds.) pp 109, Oxford University Press, New York.
49. Landry, A. (1989) Dynamic, structural, and regulatory aspects of *λ*-site-specific recombination, *Annu. Rev. Biochem. 58*, 913−949.
50. Rose, M. D., Winston, F., and Hieter, P. (1990) *Methods in Yeast Genetics*, Cold Spring Harbor Laboratory, Plainview, NY.
51. Vidal, M., Brachman, R. K., Fattaey, A., Harlow, E., and Boeke, J. D. (1996) Reverse two- and one-hybrid systems to detect dissociation of protein−protein and DNA−protein interactions, *Proc. Natl. Acad. Sci. 93*, 10315−10320.
52. Durfee, T., Bechere, K., Chen, P.-L., Yeh, S.-H., Yang, Y., Kilburn, A. E., Lee, W.-H., and Elledge, S. J. (1993) *Genes Dev. 7*, 555.
53. Schiestl, R. H. a. G. R. D. (1989) *Curr. Gen. 16*, 339−346.
54. Lakowicz, J. R. (1999) Energy transfer, in *Principles of Fluorescence Spectroscopy* (Lakowicz, J. R., Ed.) pp 367−394, Kluwer Academic/ Plenum Publishers, New York.
55. Smart, E. J., Graf, G. A., McNiven, M. A., Sessa, W. C., Engelman, J. A., Scherer, P. E., Okamoto, T., and Lisanti, M. P. (1999) Caveolins, Liquid-ordered domains, and signal transduction, *Mol. Cell. Biol. 19*, 7289−7304.
56. Edidin, M. (2001) Shrinking patches and slippery rafts: scales of domains in the plasma membrane, *Trends Cell. Biol. 11*, 492−496.
57. Pralle, A., Keller, P., Florin, E.-L., Simons, K., and Horber, J. K. H. (2000) Sphingolipid-cholesterol rafts diffuse as small entities in the plasma membrane of mammalian cells, *J. Cell Biol. 148*, 997−1007.
58. Sheets, E. D., Lee, G. M., Simons, R., and Jacobson, K. (1997) Transient confinement of a glycosylphosphatidylinositol-anchored protein in the plasma membrane, *Biochemistry 36*, 12449−12458.
59. Helmkamp, G. M. (1986) Phospholipid transfer proteins: mechanism of action, *J. Bioenerg. Biomembr. 18*, 71−91.
60. Li, H., Tremblay, J. M., Yarbrough, L. R., and Helmkamp, G. M. (2002) Both isoforms of mammalian phosphatidylinositol transfer protein are capable of binding and transporting sphingomyelin, *Biochim. Biophys. Acta 1580*, 67−76.
61. Fielding, C. J., Bist, A., and Fielding, P. E. (1998) Selective uptake of lipoprotein free cholesterol and its intracellular transport-role of caveolin, in *Intracellular Cholesterol Trafficking* (Chang, T. Y., Freeman, D. A., Eds.) pp 273−288, Kluwer Academic Publishers, Boston.
62. Brown, D. A., and London, E. (1998) Functions of lipid rafts in biological membranes, *Annu. Rev. Cell Dev. Biol. 14*, 111−136.
63. Smart, E. J., Ying, Y., Donzell, W. C., and Anderson, R. G. (1996) A role for caveolin in transport of cholesterol from endoplasmic reticulum to plasma membrane, *J. Biol. Chem. 271*, 29427−29435.
64. Uittenbogaard, A., Everson, W. V., Matveev, S. V., and Smart, E. J. (2002) Cholesteryl ester is transported from caveolae to internal membranes as part of a caveolin-annexin II lipid−protein complex, *J. Biol. Chem. 277*, 4925−4931.
65. Fuchs, M., Lammert, F., Wang, D. Q. H., Paigen, B., Carey, M. C., and Cohen, D. E. (1998) Sterol carrier protein-2 participates in hypersecretion of biliary cholesterol during cholesterol gallstone formation in genetically gallstone susceptible mice, *Biochem. J. 336*, 33−37.
66. Cohen, D. E., Leonard, M. R., and Carey, M. C. (1994) In vitro evidence that phospholipid secretion into bile may be coordinated

intracellularly by the combined actions of bile salts and the specific phosphatidylcholine transfer protein of liver, *Biochemistry 33*, 9975−9980.
67. Wustner, D., Herrmann, A., Hao, M., and Maxfield, F. R. (2002) Rapid nonvesicular transport of sterol between the plasma membrane domains of polarized hepatic cells, *J. Biol. Chem. 277*, 30325−30336.
68. Stolowich, N. J., Petrescu, A. D., Huang, H., Martin, G., Scott, A. I., and Schroeder, F. (2002) Sterol carrier protein-2: structure reveals function, *Cell. Mol. Life Sci. 59*, 193−212.
69. Pfanner, N., Orci, L., Glick, B. S., Amherdt, M., Arden, S. R., Malhotra, V., and Rothman, J. E. (1989) Fatty acyl CoA is required for budding of transport vesicles from *Golgi cisternae*, *Cell 59*, 95−102.
70. Pfanner, N., Glick, B. S., Arden, S. R., and Rothman, J. E. (1990) Fatty acylation promotes fusion of transport vesicles with *Golgi cisternae*, *J. Cell Biol. 110*, 955−961.
71. Puglielli, L., Rigotti, A., Greco, A. V., Santos, M. J., and Nervi, F. (1995) Sterol carrier protein-2 is involved in cholesterol transfer from the endoplasmic reticulum to the plasma membrane in human fibroblasts, *J. Biol. Chem. 270*, 18723−18726.
72. Goligorsky, M. S., Li, H., Brodsky, S., and Chen, J. (2002) Relationships between caveolae and eNOS: everything in proximity and proximity of everything, *Am. J. Physiol. 283*, F1−F10.
73. Cockcroft, S. (1998) Phosphatidylinositol transfer proteins: a requirement in signal transduction and vesicle traffic, *BioEssays 20*, 423−432.
74. Liu, P., Rudick, M., and Anderson, R. G. W. (2002) Multiple functions of caveolin-1, *J. Biol. Chem. 277*, 41295−41298.
75. Gallegos, A. M., McIntosh, A. L., Atshaves, B. P., and Schroeder, F. (2004) Structure and cholesterol domain dynamics of caveolae, *Biochem. J.*, in press.

BI035914N